IEEE Access
Multidisciplinary ⋮ Rapid Review ⋮ Open Access Journal

Received 21 February 2023, accepted 2 March 2023, date of publication 8 March 2023, date of current version 14 March 2023.

Digital Object Identifier 10.1109/ACCESS.2023.3253868

RESEARCH ARTICLE

PoxNet22: A Fine-Tuned Model for the Classification of Monkeypox Disease Using Transfer Learning

FARHANA YASMIN[1], MD. MEHEDI HASSAN[2], (Member, IEEE), MAHADE HASAN[1], SADIKA ZAMAN[3], CHETNA KAUSHAL[4], WALID EL-SHAFAI[5,6], AND NAGLAA F. SOLIMAN[7]

[1]Department of Computer Application Technology, Changzhou University, Changzhou 213164, China
[2]Computer Science and Engineering Discipline, Khulna University, Khulna 9208, Bangladesh
[3]Department of Computer Science and Engineering, North Western University, Khulna 9000, Bangladesh
[4]Chitkara University Institute of Engineering and Technology, Chitkara University, Punjab 140401, India
[5]Security Engineering Laboratory, Computer Science Department, Prince Sultan University, Riyadh 11586, Saudi Arabia
[6]Department of Electronics and Electrical Communications Engineering, Faculty of Electronic Engineering, Menoufia University, Menouf 32952, Egypt
[7]Department of Information Technology, College of Computer and Information Sciences, Princess Nourah bint Abdulrahman University, Riyadh 11671, Saudi Arabia

Corresponding authors: Md. Mehedi Hassan (mehedihassan@ieee.org), Walid El-Shafai (eng.waled.elshafai@gmail.com), and Naglaa F. Soliman (nfsoliman@pnu.edu.sa)

This work was supported by the Princess Nourah bint Abdulrahman University, Riyadh, Saudi Arabia, through Researchers Supporting under Project PNURSP2023R66.

ABSTRACT Officials in the field of public health are concerned about a new monkeypox outbreak, even though the world is now experiencing an epidemic of COVID-19. Similar to variola, cowpox, and vaccinia, an orthopoxvirus with two double-stranded strands causes monkeypox. The present pandemic has been propagated sexually on a massive scale, particularly among individuals who identify as gay or bisexual. In this instance, the speed with which monkeypox was diagnosed is the most important aspect. It is possible that the technology of machine learning could be of significant assistance in accurately diagnosing the monkeypox sickness before it can spread to more people. This study aims to determine a solution to the problem by developing a model for the diagnosis of monkeypox through machine learning and image processing methods. To accomplish this, data augmentation approaches have been applied to avoid the chances of the model's overfitting. Then, the transfer-learning strategy was utilized to apply the preprocessed dataset to a total of six different Deep Learning (DL) models. The model with the best precision, recall, and accuracy performance matrices was selected after those three metrics were compared to one another. A model called ''PoxNet22'' has been proposed by performing fine-tuning the model that has performed the best. PoxNet22 outperforms other methods in its classification of monkeypox, which it does with 100% precision, recall, and accuracy. The outcomes of this study will prove to be extremely helpful to clinicians in the process of classifying and diagnosing monkeypox sickness.

INDEX TERMS Monkeypox, data augmentation, transfer learning, classification, PoxNet22.

I. INTRODUCTION

Public health professionals are worried about a new monkeypox outbreak despite the global COVID-19 epidemic. Monkeypox is an orthopoxvirus with two double-stranded strands like variola, cowpox, and vaccinia. Dormice, tree squirrels, Gambian pouched rats, and rope squirrels spread monkeypox. The more dangerous monkeypox viral lineage is found in Central and West Africa. Numerous cases of the present outbreak result from sexual transmission, particularly

The associate editor coordinating the review of this manuscript and approving it for publication was Anandakumar Haldorai.

in gays and bisexuals. The virus can spread by bodily fluids, scabs, infected wounds, and sharing beds or clothing. Rash, fever, lymphadenopathy, and flu. Up till the wounds have healed, the prodrome or rash is spreadable. Active monkeypox is indicated by viral DNA found in vesicle crusts or ulcers [1]. On May 17, 2022, the Laboratory Response Network (LRN) of the Massachusetts Department of Public Health (MDPH) employed real-time PCR to confirm orthopoxvirus DNA in lesion swabs from a Massachusetts person. On May 18, CDC real-time PCR tests revealed that the patient had monkeypox from the West African subclade. There are no endemic hotspots in the 28 countries and territories having laboratory-confirmed cases of monkeypox. A phone center helped states on May 19 with monkeypox evaluation, clinical diagnosis, and orthopoxvirus testing. By May 31st, this study had uncovered 17 US instances [2]. More than 48,000 instances of the monkeypox virus have been reported in less than 4 months, with a total of 13 fatalities [3]. The United States is now conducting a Randomized Controlled Trial (RCT) to assess the effectiveness and safety of tecovirimat as a monkeypox therapy. The Centers for Disease Control and Prevention (CDC) and the Food and Drug Administration (FDA) have accelerated the extended access strategy while RCTs are being prepared since the hazards of monkeypox and the safety of tecovirimat in healthy humans and animal models are both well-known. With the help of healthcare professionals, researchers will use this technology to keep these treatments up to date. The clinical features of the pandemic need the RCTs to assess tecovirimat's effectiveness and safety in treating monkeypox. According to the CDC, FDA, and NIH, tecovirimat may be used humanely until RCTs demonstrate their safety and efficacy [4]. It is now more crucial to distinguish monkeypox from other orthopoxviruses by its categorization.

Machine learning (ML), a discipline within artificial intelligence, is relatively new but has already demonstrated significant potential in various applications. These include industrial applications, medical imaging, and disease detection [38], as well as applications that help individuals make decisions [35], [37]. Machine-learning-enabled imaging systems are valuable by medical practitioners as essential tools for conducting rapid evaluations that are accurate and secure [36]. For large-scale COVID-19 classification, this work [5] proposes layered ensemble meta-classifiers and feature fusion powered by deep learning. Kernel principal component analysis reduced the dimensionality of the data and removed features from the top layer in pre-trained models based on EfficientNet (global average pooling). Stacked ensemble meta-classifiers categorized everything in the end. SVM and random forest predictions were integrated before the second stage. The COVID-19 status of CT and CXR data is determined by second-stage logistic regression. And the suggested model outperformed current approaches for the diagnosis. 1345 CT scans were used to extract deep features using ResNet-50, ResNet-101, AlexNet, Vgg-16, Vgg-19, GoogLeNet, SqueezeNet, and Xception. With the use of test images, these detailed properties are assessed using classification algorithms like SVM, k Nearest Neighbor, Random Forest, Decision Trees, and Naive Bayes (NB). Application data showed that SVM and ResNet-50 performed the best. As an additional decision support system, the efficient deep learning model and classification strategy employed in this work can minimize the need for extra COVID-19 testing [6]. Ten learnable layers—nine convolutional and one fully connected—make up the model [7]. Employing deep learning to find COVID-19 on chest radiographs. Chest radiographs can be classified as normal, positive, or pneumonia using a fine-grained COVID-19 classification experiment. Moreover, a COVID-19 Radiography Database is used to evaluate the special CovidDetNet deep learning model. In dataset experiments, the proposed CovidDetNet model fared better than the alternatives. They provide a cutting-edge method for examining chest X-ray pictures in order to detect COVID-19 and pneumonia. There are three steps in the method [8]. The conditional generative adversarial network (C-GAN) separates unprocessed X-ray data to produce lung pictures. The second stage involves sending segmented lung images to a special pipeline that extracts distinguishing traits through keypoint extraction and training deep neural networks (DNN). The last step involves classifying COVID-19, pneumonia, and normal lung pictures using ML models. Comparisons are made between the classification performance of DNN-ML-DNN architectures. While evaluating classification accuracy, the VGG-19 model with the binary robust invariant scalable key points (BRISK) technique produced the best results.

Furthermore, to identify prostate cancer in ultrasonography and MRI images, this study [9] suggests deep learning methods. Applying adjustable-layer pre-trained deep learning models to datasets. The best test model has 97% US image accuracy and 80% MRI image accuracy. The best classification model extracted fusion model characteristics. A fusion model is developed for the MRI dataset using the best pre-trained feature extractor and shallow machine learning techniques (e.g., SVM, Adaboost, K-NN, and Random Forests). This approach of data fusion raises the accuracy of MRI datasets from 80% to 88%. Using ultrasound pictures to identify breast cancer, the proposed [10] framework has five main steps: data augmentation, a pre-trained DarkNet-53 model, transfer learning, and feature extraction from the global average pooling layer. The best features are selected using reformed differential evaluation (RDE) and reformed gray wolf (RGW). The best accuracy was 99.1% using an enhanced Breast Ultrasound Imagery (BUSI) dataset. A deep learning training technique is used to explicitly instruct the network to concentrate on and accurately recognize regions with cancerous image regions. Gradient-weighted class activation mapping by Selvaraju et al. described CNNs. Pictures from their own mobile oral screening device and two-step data augmentation were used to train Li et al.'s inference

network (GAIN). GAIN categorizes, trains, and harvests attention using bounding box networks. These attention maps were used in conjunction with the GAIN training architecture as reliable priors to produce attention maps with improved segmentation [11]. The most effective genes for gene expression in diverse illnesses are identified using soft ensembling and a novel deep neural network. The feature selection strategy selects wrapper genes using three different methods and ranks them using the k-nearest neighbor algorithm to provide a generalizable and error-free model. A stacked deep neural network correctly identified three datasets with accuracies of 97.51%, 99.6%, and 96.34% [12].

When this article was created, only a handful of articles showed how image processing and machine learning methods might be used to diagnose monkeypox. These articles served as the sources for the information in this article. While this story was being written, these papers surfaced and were covered. Unfortunately, the absence of a publicly accessible dataset for training and testing hampered the development of a system for the image-based diagnosis of monkeypox. This was a direct effect of the virus's fairly recent dissemination to substantial populations in a number of different countries throughout the world.

This study aims to find a solution by developing a model for the diagnosis of monkeypox using image processing and machine learning techniques. That includes Related Work, Experimentation Environment, Methodology, Data Collection, Data Preprocessing, Data Augmentation, Train Test Split, Applied Models, Select Best Model, Proposed Model, Result Analysis, Ablution Study, Discussion, Compare with Existing Works, and Conclusion. The significant implications of this research are:

- The dataset was preprocessed to improve image quality.
- Performing data augmentation to reduce the chance of the model's overfitting.
- Applying six different models on the dataset.
- Comparing the performance of those models to identify the best model.
- Proposing a model PoxNet22 by fine-tuning the InceptionV3 model to classify monkeypox among others pox more precisely.
- Analyzing how the PoxNet22 model performed in comparison to earlier research.

Although there have only been a very small number of papers published that exclusively work on the classification of monkeypox using artificial intelligence, this study employed two open-sourced monkeypox and chickenpox digitized skin images. A two-dimensional CNN with four convolutional layers was used. They compared the performance of their suggested model to cutting-edge deep-learning algorithms for the detection of skin lesions. Their CNN model outperformed all DL models in test accuracy, scoring 99.60%. Precision, recall, and F1 score were weighted and averaged at 99.00%. Alex Net outperformed trained models with an accuracy of 98.00% [39]. This study used the transfer learning model and hyperparameters to develop a hybrid function learning model. This is incorporated in the MobileNetV3-s, EfficientNetV2, ResNET50, Vgg19, DenseNet121, and Xception custom models. AUC, accuracy, recall, loss, and F1-score were all compared in this study. With a 0.98 average F1-score, 0.99 AUC, 0.96 accuracy, and 0.97 recall, the improved hybrid MobileNetV3-s model surpassed the opposition [40]. However, artificial intelligence has been utilized more frequently in recent years for image classification across a variety of image formats. In light of this, further explanation is presented in the subsequent section.

II. RELATED WORK

The research work that uses only images for experiments on the topics such as monkeypox, COVID-19, MRI, and cancer was discussed in this section. In which the literature that is related to our study has been reviewed. When we reviewed those works of literature, we took into consideration the study methodologies and the findings of the investigations as follows.

The suggested techniques by the authors [13] include transfer learning, meta-heuristic optimization, and multi-layer neural network parameter optimization. Meta-heuristic optimization strategies include the Al-Biruni Earth radius, sine-cosine, and particle swarm optimization approaches. Deep learning by GoogleNet extracts features. These methods offer a fresh binary hybrid algorithm and a hybrid method for optimizing neural network parameters. Algorithms are evaluated using a public dataset. The optimization of the choice of the monkeypox classification feature was assessed using ten criteria. 98.8%, on average, were correct in their classifications. This study [14] is aimed at 13 deep learning (DL) models that have been trained to identify monkeypox. They all receive common custom layers and undergo analysis using four well-known metrics: Precision, recall, accuracy, and F1 score. After a majority vote on probabilistic outcomes, they assemble the best DL models. They reach averages of 85.44%, 85.47%, 85.40%, and 87.13% for Precision, Recall, F1-score, and Accuracy, respectively, using a public dataset and the proposed ensemble technique. Ali et al. [15] The ''Monkeypox Skin Lesion Dataset (MSLD)'' contains images of lesions caused by measles, chickenpox, and monkeypox. The majority of images come from news sources, blogs, and open case reports. A 3-fold cross-validation experiment's sample size is increased through data augmentation. Then, diseases like monkeypox are classified using pre-trained deep-learning models like VGG-16, ResNet50, and InceptionV3. A trio of models was constructed. The accuracy of ResNet50 is 82.96%, that of VGG16 is 81.48%, and that of the ensemble system is 79.26%.

Additionally, the authors [16] proposed a COVID-19 classification model that has been tested on 7132 chest x-ray (CXR) images from public sources. Gradient-weighted Class Activation Mapping (Grad-CAM), Local Interpretable Modelagnostic Explanation (LIME), and Shapley Additive Explanation are used to interpret and explain the results to make them more understandable (SHAP).

Convolution characteristics are first extracted in order to gather comprehensive object-based data. The black-box method of the DL model is next examined using shapely values from SHAP, predictability findings from LIME, and heatmap from Grad-CAM. As a result, the 10-fold cross-validation yields an average test accuracy of 94.31% and a validation accuracy of 94.54%. Loey et al. [17] the identification of chest X-rays is performed using a novel Bayesian optimization-based convolutional neural network (CNN) model. The model is divided into two segments. CNN first learns and extracts deep features. A Bayesian-based optimizer, the second component, modifies CNN hyperparameters using an objective function. 10,848 images were included in the expansive, balanced collection. Initial ablation research contrasted three ablation scenarios with Bayesian optimization. The three scenarios were compared using convergence charts and accuracy. Optimal architecture determined by Bayesian search was 96% accurate. The approach in this paper is to use deep learning to distinguish between COVID-19 infection and other diseases. EfficientNetB1, NasNetMobile, and MobileNetV2 are three pre-trained models that categorize COVID-19. To train deep learning models, the augmented dataset is used performance of the deep learning model, and hyperparameters are improved by this study [18]. The classification head's regularization improves performance. Methods are evaluated based on a range of performance metrics. EfficientNetB1's regularized classification head outperforms the competition. The method can classify COVID-19, viral pneumonia, lung opacity, and normal with a 96.13% accuracy rate. They employed [19] the Sobel, Laplacian of Gaussian (LoG), and Gabor filters to extract more characteristics from the sparse data. Many deep transfer models were used to assess and compare the suggested tactic. The models were trained using 360 COVID-19 CXR pictures. The accuracy growth of the Gabor filter bank, which increased by 32% during 45 epochs, is the best in terms of assessment criteria value growth. The proposed DenseNet-201 model was tested against ten COVID-19 detection techniques. Our advanced COVID-19 detection technique has a two-class classification accuracy of 98.5%. [20] Kogilavani et al. Deep learning techniques are used to identify COVID-19 patients in CT scans. Deep learning methods have been developed for COVID-19. The CNN architectures VGG16, DeseNet121, MobileNet, NASNet, Xception, and EfficientNet are used in this work. There have been 3873 CT scans, both ''COVID'' and ''Non-COVID.'' separate datasets were used for the test and validation phases. Accuracy was 96.68% for VGG16, 97.53% for DenseNet121, 96.38% for MobileNet, 89.51% for NASNet, 92.47% for Xception, and 80.19% for EfficientNet. The analysis demonstrates the superior accuracy of the VGG16 architecture. In this study [21], a multi-image augmented convolutional neural network is used to assess CT and X-ray images of coronavirus suspects to identify COVID-19 (CNN). Multi-image augmentation provides beneficial CNN model training examples by using edge information from edged images. This method generates a model with a classification accuracy of 98.97% for X-ray images and 95.38% for CT scan images. Multi-image enhanced X-ray images have a specificity and sensitivity of 98.88% and 99.07%, compared to 95.78% and 94.78% for CT scan images. Using fuzzy logic-based deep learning, the CXR pictures of patients with interstitial pneumonia unrelated to Covid-19 were separated from those of patients with Covid-19 pneumonia. The CovNNet model [22] recovers a number of significant properties from CXR pictures and fuzzy images using fuzzy edge detection. As compared to benchmark deep learning techniques, experimental results show that adding a deep network input to an MLP with CXR and fuzzy features improves classification performance by 81%.

Also, this study [23] classifies multi-class glioma tumors using deep learning-based traits and the Support Vector Machine (SVM) classifier. Deep convolution neural networks mine data from MRI images for an SVM classifier. The proposed technique accurately diagnosed the four glioma classes, with a 96.19% accuracy rate for HGG in FLAIR and 95.46% for LGG in T2 (Edema, Necrosis, Enhancing, and Non-enhancing). The recommended solution outperformed comparable techniques in the literature when applied on the same BraTS dataset. This study outperforms previously trained GoogleNet and LeNet models on the same dataset. The brain tumor is located in this study [24] by examining hyperspectral images. Using k-nearest neighbor and k-means clustering, the tumor is located. The firefly algorithm maximizes k for both approaches. The use of optimization techniques lessens the need for human calculation of K's ideal value for brain partitioning. The multilayer feedforward neural network labels different parts of the brain. The proposed method outperforms hybrid and parallel k-means clustering in terms of accuracy due to its greater peak signal-to-noise ratio and lower mean absolute error value. The model fared better than earlier approaches, with accuracy, sensitivity, and specificity of 96.47%, 96.32%, and 98.24%, respectively. The authors [25] have categorized FLAIR, T1, T2, and T1CE tumors using deep learning. The dataset was normalized and sent to ResNet101. ResNet101's classification of brain cancers has improved. Redundancy plagues the procedure. Redundancy raises labor expenses and lowers computational accuracy. Particle swarm optimization and differential evaluation are used to identify the optimum attributes. Serially fusing faultless feature vectors results in a single-fused feature vector. On this fused vector, PCA is used to get the best feature vector. The ongoing evaluation of multiple cancer classifiers makes use of this updated feature vector. The method increased medium neural network prediction time by 25.5x while boosting accuracy by 94.4%.

The authors' [26] generative adversarial model uses unrelated cancer data to identify the target to enhance classification performance for classifying cancer. They further stabilize model training and improve the samples' caliber by using

the reconstruction loss. According to experimental results, our data are classified more accurately than data produced by GAN because the model's mean absolute error for the cancer gene is 19.3% lower than DC-GAN's. Our model's classification accuracy is 92.6%, which is 7.6% higher than the model's accuracy when no produced data is used. Mixed ensemble learning is used in the prediction analysis to classify breast cancer. Blended ensemble model [27] base learners. Ensemble Learning performs 98.14% better than simple learning. This work presents [28] a melanoma classifier based on DCNN. DCNN layers extract low- to high-level skin characteristics in a distinctive way. A lightweight, simpler DCNN will more accurately classify melanoma skin cancer than it is by present techniques. Dermoscopic carcinoma images from the International Skin Imaging Collaboration data stores were used in this investigation. On the ISIC 2016, 2017, and 2020 datasets, the proposed DCNN classifier outperforms cutting-edge networks with accuracies of 81.41%, 88.23%, and 90.42%.

Now that we have established that, let's briefly discuss the approach that was taken in this research. This will be covered in more detail in the methodology section that is presented after.

III. EXPERIMENTATION ENVIRONMENT

We use the libraries Keras, Tensorflow, and OpenCV 2 to simulate the image datasets. In order to conduct our experiment, we utilized Google Colab. The language that was utilized was Python. Where 11.4 was the version of CUDA, and 470.82.01 was the version of the Nvidia-semi driver. In addition to it, we employ a Tesla P100-PCIE GPU. Furthermore, we used Pandas for data analysis and NumPy for numerical calculations.

IV. METHODOLOGY

This study was completed by carrying out the nine primary sections. The specifics of the dataset's description are presented and discussed in part of the ''Data Collection'' section. In addition to that, the data set's origin has been dissected in a detailed manner. In the section titled ''Data Preprocessing,'' the overall image quality of the dataset has been enhanced using a variety of image preparation methods. The dataset has been divided into a train set and a test set in the section titled ''Train Test Split'' to run the experiment on both of them. In addition, in the 'Data Augmentation' section, data augmentation has been carried out to reduce the possibility of the model overfitting. This resulted in a considerable rise in the overall number of images inside the collection. Within the 'Applied Model' section, there are a total of six distinct models that have been used to analyze the dataset. The model with the best overall performance was chosen after evaluating all of the models in the ''Select Best Model'' section and picking the one that performed the best overall. After that, in the area labeled ''Propose Model,'' a model called PoxNet22 was proposed by fine-tuning the model that performed the best, which was known as ''InceptionV3.'' The 'Result Analysis' section has then gone on to discuss the performances of the PoxNet22 model. Here, a quick description of the model ablution study and the impact of data augmentation on the model is given. Finally, to classify monkeypox using artificial intelligence, the results of PoxNet22 have been evaluated and contrasted with those of previously published work. Figure 1 shows the procedure flow diagram for this study.

Now the working process of this study is being initiated by the dataset section to discuss the attributes of the dataset in the following manner.

V. DATASET

In this study, a total of 3,192 images from the Kaggle ''Monkeypox Skin Lesion Dataset (MSLD)'' [15] are evaluated. MSLD image dataset has 3 folders. The ''Augmented Images'' folder has been employed to evaluate this study. Considering how rapidly monkeypox spreads, early detection is essential. However, confirmatory Polymerase Chain Reaction (PCR) tests and other biochemical diagnostics are not widely available in considerable quantities. Therefore, to create the MSLD, images from various web-scraping sources, including news portals, websites, and publicly available case reports, are gathered and analyzed. To differentiate monkeypox patients from associated non-monkeypox cases was the major goal of the ''Monkeypox Imaging Lesion Dataset.'' In addition to the ''Monkeypox'' class, the ''Others'' class was used to perform binary classification on photos of chickenpox and measles skin lesions because of their similarity to the rash and pustules of monkeypox in their early stages. The categories ''Monkeypox'' and ''Others'' include 1428 and 1764 photos, respectively. The description of the dataset is presented in Table 1.

Due to the fact that the dataset is not yet in its final state for the simulation, it is necessary to carry out a few data preparation methods to make the dataset more compatible with the models outlined below.

VI. DATA PREPROCESSING

During the preprocessing stage of the data, various methods were utilized, such as low-contrast pictures, contrast stretching, histogram equalization, and adaptive equalization. The dataset is divided into two categories, ''monkeypox'' and ''others'' as mentioned earlier. As a result, the data preparation procedure was applied to each class individually. The contexts in which there is a low contrast between the image and the background make it more difficult for models to decide whether image borders are clear. In order to increase the range of intensity values that the images can include, contrast stretching was applied to the images. Histogram equalization was then performed, which ultimately led to the most frequent intensity values being distributed in a manner that was consistent throughout the grid. In addition to this, adaptive equalization helps to improve the contrast in the surrounding area, and that is the benefit of using it. Figure 2 illustrates (a) the preprocessing data result of the

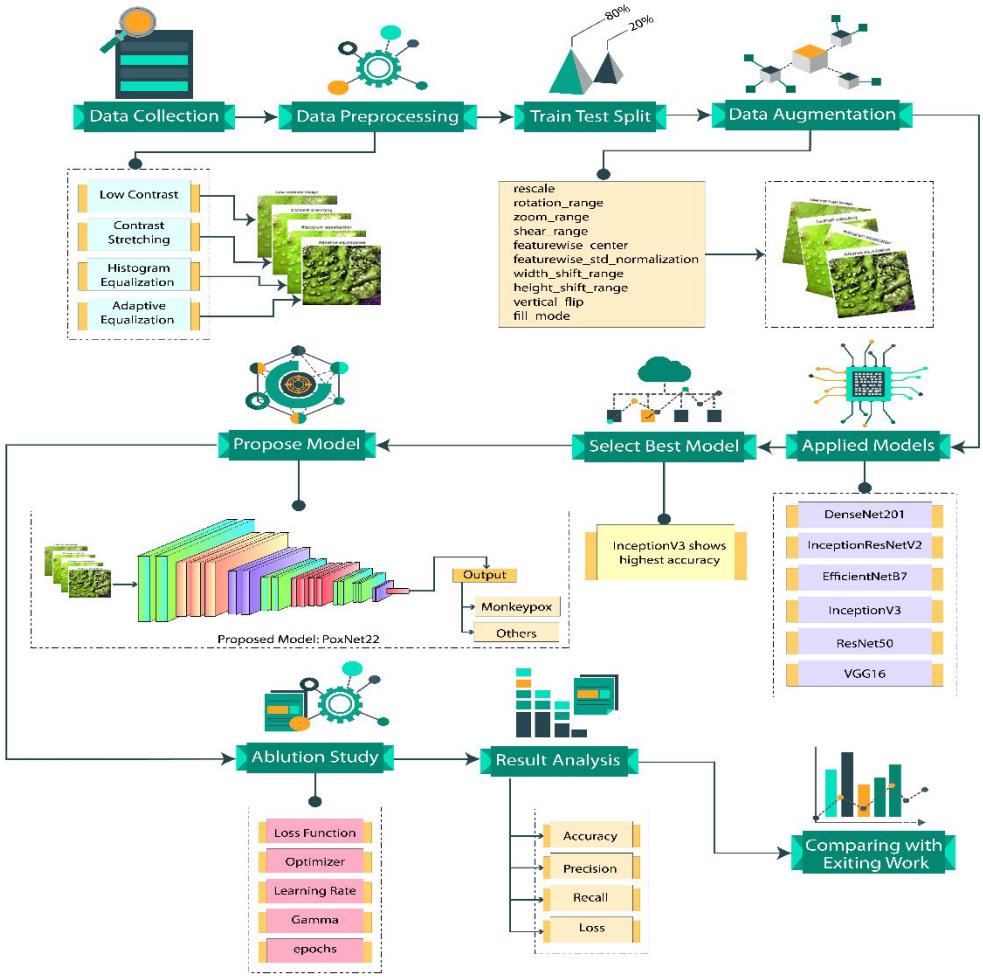

FIGURE 1. The Working flow Chart of This Study. Nine core sections completed this study. Where the component of "Data Collection" discusses the dataset's description. "Data Preprocessing" uses several image preprocessing methods to increase dataset image quality. The dataset has been split into a train set and a test set under the "Train Test Split" section to experiment on both sets. In the "Data Augmentation" phase, data was augmented to reduce model overfitting. Boosting the collection's image count. Six dataset-analyzing models are listed in the "Applied Model" section. After reviewing all models in the "Select Best Model" section, the best overall model was chosen. In the "Propose Model" section, the best model, "InceptionV3," was fine-tuned to create PoxNet22. 'The "Result Analysis" section then discussed PoxNet22 model performance. The model's ablution study and data augmentation effects were briefly detailed here. Finally, PoxNet22 results were compared to prior work to classify monkeypox using artificial intelligence.

TABLE 1. Dataset description.

Name	Description
Total Number of Images	3192
Dimension	224×224
Data Set Type	Imbalance
Total Number of Classes	2
Monkeypox	1428
Others	1764

"Monkeypox" class and (b) the preprocessing data result of the "Others" class.

The dataset is now ready to be placed to use in simulation as a result of the data preprocessing operation having been carried out and successfully finished. The dataset was originally split into a train set and a test set before the simulation began using the method that will be covered in more detail in the following section.

VII. TRAIN TEST SPLIT

A train set and a test set were created from the dataset through processing, and they have split apart during the train-test split. Eighty percent of the photographs in the training set were chosen at random, while only twenty percent of the images in the testing set were used. As a result, whereas the test set only has 639 total images, the train set has a total of 2553 images. Table 2 provides a summary of the train test split dataset's description.

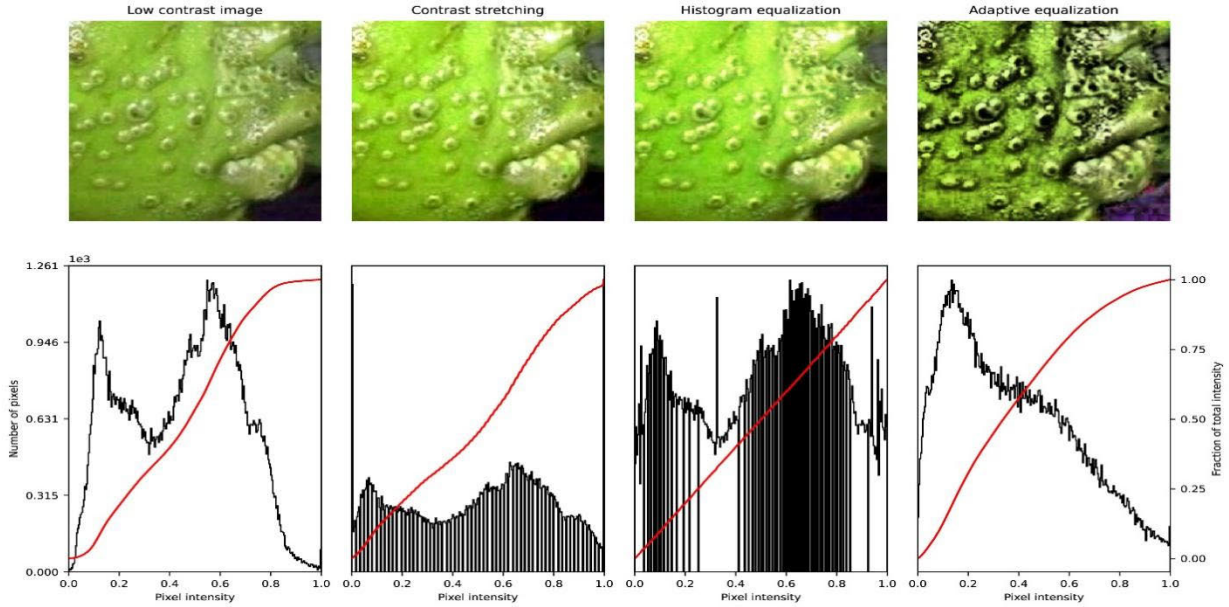

(a)

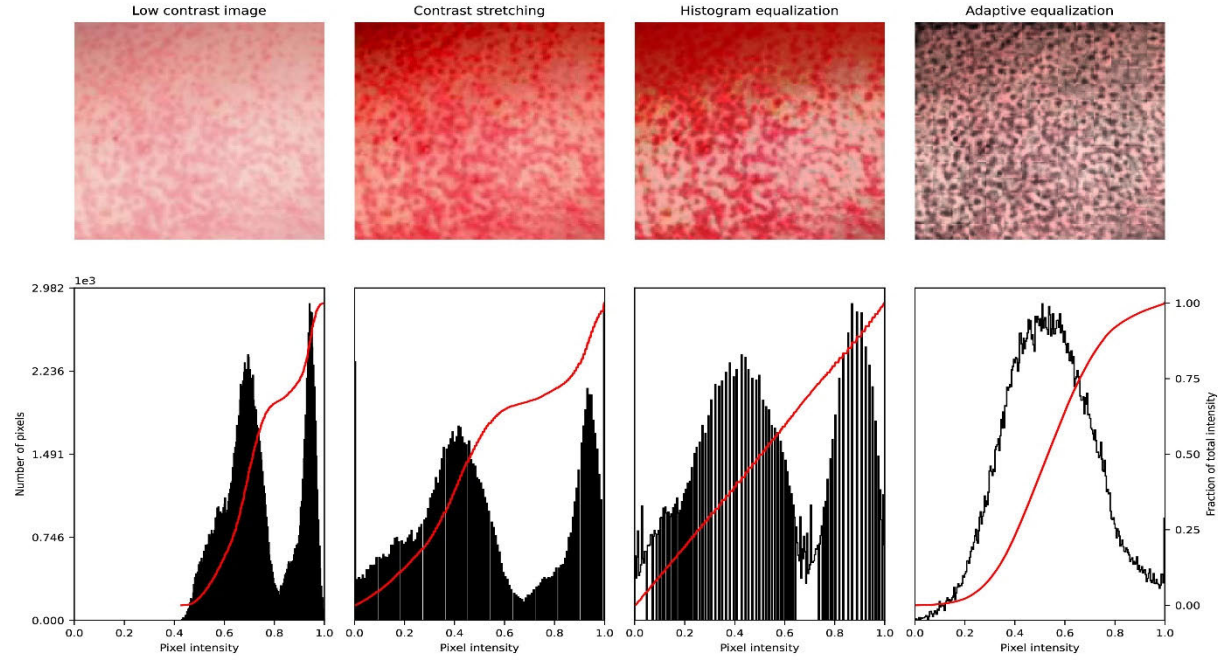

(b)

FIGURE 2. Illustrates (a) the preprocessing data result of the "Monkeypox" class; and (b) the preprocessing data result of the "Others" class. The first demonstrates a low-contrast image, the second demonstrates contrast stretching, the third demonstrates histogram equalization, and the fourth and final demonstrates adaptive equalization, each displaying the pixel intensity and number of pixels, and fraction of total intensity that corresponds to it.

The full dataset includes a total of 3,192 images when it is taken into consideration, which is not nearly enough to make the model extremely precise and obtain the result that was supposed to be accomplished. As a direct result of this, the augmentation of the data that will be the focus of the discussion in the following part has been carried out.

VIII. DATA AUGMENTATION

To ensure that the training dataset contained correct data and information, throughout the whole data augmentation procedure, the rescaled value was kept at 1./255. After that, the rotation's range was modified to 20, which allowed the images to be turned between 0 and 20 degrees in

TABLE 2. Train test split dataset description.

Name	Description
Train set percentage	80%
Test set percentage	20%
Number of Train set images	2553
Number of Test set images	639
Total Number of Images	3192

any direction. After this one, the zoom range was increased to 0.2 so that it would allow for a 20% in/out zoom. It was performed in preparation for the next one. It was then carried out to facilitate the adjustment at a later time. Additionally, the shear range was adjusted to 0.2 so that a total of 20% could share the image. This was applied so that the image would be more flexible. In addition, the image means for the entire dataset was altered to be equal to 0 by setting the value of the feature-wise center parameter to True. This has been performed to conclude the transformation. After completing this stage of the process, the value for the feature-wise std normalization option was opted to be True. Because of this, the inputs were able to be divided according to the dataset's standard deviation. After that, the width and height shift ranges were both set to 0 to move the image along the X and Y axes by 0% and 0%, respectively. It was also executed to ensure that the image can be featured using the specified dimensions. During this time, the configuration for the vertical flip was adjusted to ''False.'' In addition to that, the ''nearest'' setting was set as the one to utilize for the fill mode. Last but not least, the rescaled value for the test dataset was set to 1./255. An overview of the data augmentation description can be seen in Table 3.

TABLE 3. Summarized data augmentation description.

Name	Description
rescale	1./255
rotation_range	20
zoom_range	0.2
shear_range	0.2
featurewise_center	True
featurewise_std_normalization	True
width_shift_range	0
height_shift_range	0
vertical_flip	False
fill_mode	'nearest'

Figure 3 illustrates (a) the data augmentation result of the ''Monkeypox'' class and (b) the data augmentation result of the ''Others'' class, where some augmentation approaches are taken into consideration.

The training dataset was expanded, increasing the number of images from 2553 to 3071. Moreover, the test dataset's image count rose from 639 to 1157. Overall, there are currently 4,228 images in total. Therefore, the dataset is prepared to be used in the simulation.

IX. APPLIED MODELS

In the process of this study, a total of six different models were used at various points. DenseNet201, InceptionResNetV2, EfficientNetB7, InceptionV3, ResNet50, and VGG16 are the names of these models respectively. To apply all of the models to our dataset utilizing the method that is outlined further down below, the following procedures need to be carried out.

A. DenseNet201

There are 201 layers in the ''DenseNet-201,'' a convolutional neural network [29]. A modern pre-trained DenseNet201 neural network categorized the dataset into ''Monkeypox'' and ''Others'' in this investigation. Transfer learning extracted features from DenseNet201 after adding two layers. GlobalAveragePooling2D and Dense were optimized for performance. Two loss matrices corrected dataset inconsistencies. The binary focal loss and the binary cross entropy are the two matrices exhibiting these. Table 4 and Table 5 give brief explanations of the fine-tuning of the parameters for binary cross entropy and binary focal loss, respectively. These explanations are presented in the tables.

In the beginning, as can be seen in Table 4, For the DenseNet201 model, binary cross-entropy was chosen as the loss function. The learning rate was set to 0.001, and Adam chose to act as the optimizer. Epochs were set to ten. The loss function for the DenseNet201 model was then once more changed in accordance with Table 5 to BinaryFocalLoss with gamma 2.0, the optimizer Adam, and the learning rate 0.001. Epochs had a value of 10. Figures 4(a) and (b) show, respectively, the model's performance using the binary cross entropy loss function and the binaryFocalLoss loss function.

Figure 4 illustrates the model's performance, with the color red showing the model's losses. The extent to which a line in the graph is colored green can also indicate how accurate the model is. In addition to that, the color blue is shown to be able to represent the degree of precision that the model possesses. In addition, the recall of the model is represented by the color cyan. It is obvious that the performance of the binary focal loss function is superior to that of the binary cross entropy loss function when compared to the performance of the binary cross entropy loss function. This is demonstrated by the fact that. This is due to the inherently imbalanced character of the dataset.

B. InceptionResNetV2

A convolutional neural network known as InceptionResNetV2 was trained using more than a million photos from the ImageNet collection, and it was then used to classify images [30]. The network, which consists of 164 layers, can categorize photos into 1000 different types of things.

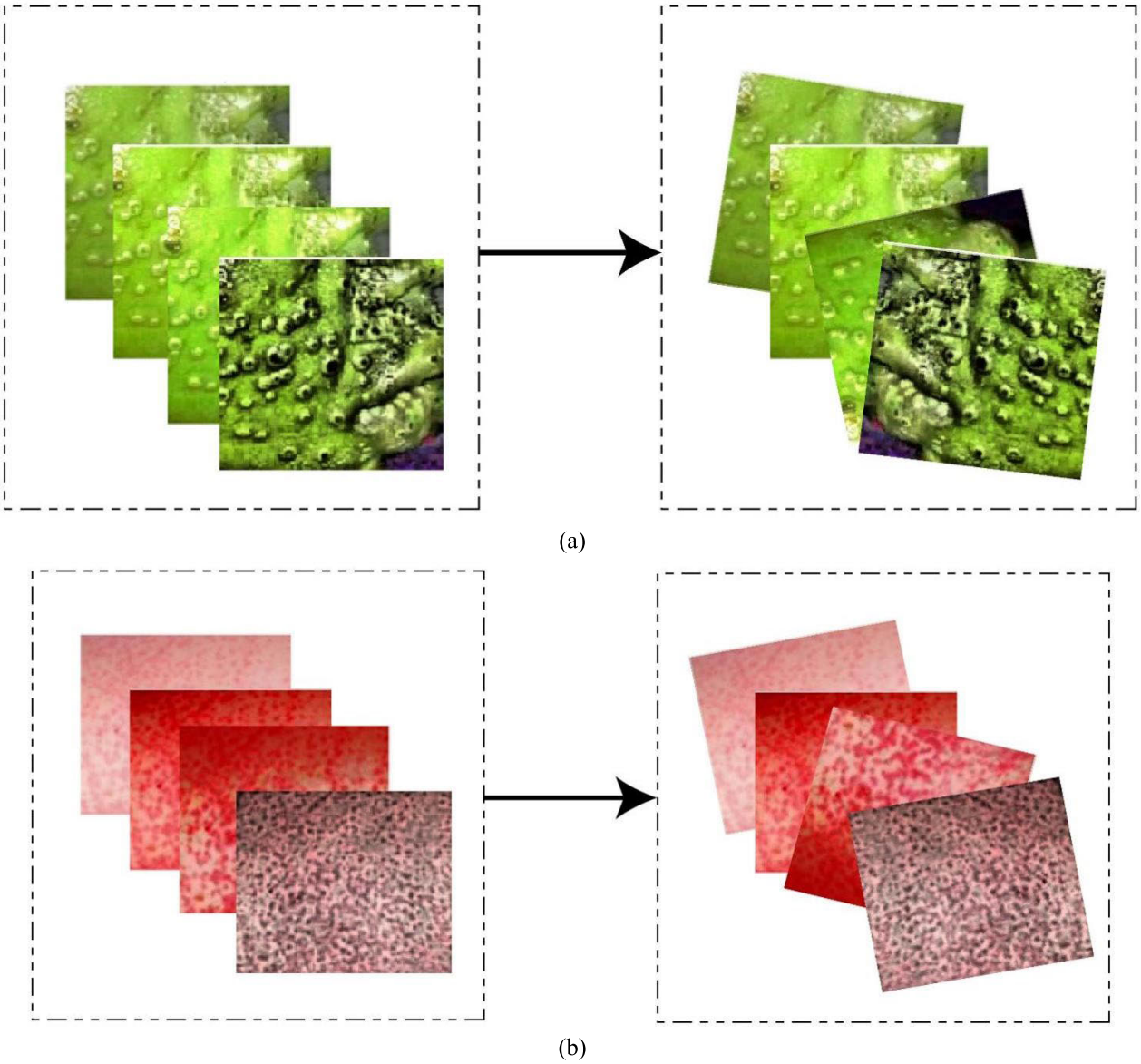

FIGURE 3. Illustrates (a) the data augmentation result of the "Monkeypox" class; and (b) the data augmentation result of the "Others" class.

TABLE 4. Summarized fine-tuned parameters description of DenseNet201's binary cross entropy.

Name	Description
Loss	binary_crossentropy
Optimizer	Adam
Learning Rate	0.001
epochs	10

TABLE 5. Summarized fine-tuned parameters description of DenseNet201's binary focal loss.

Name	Description
Loss	BinaryFocalLoss
Gamma	2.0
Optimizer	Adam
Learning Rate	0.001
epochs	10

In Tables 6 and Table 7, respectively, the settings for binary cross entropy and binary focal loss are adjusted. The tables that follow offer further information and specifics about these adjustments.

Table 6's information demonstrates that the loss function for the InceptionResNetV2 model was binary cross-entropy. Adam was given the optimizer role, and the learning rate was changed to 0.001. The epochs were represented by the number 10. After that, the InceptionResNetV2 model's loss function was changed to BinaryFocalLoss with gamma 2.0,

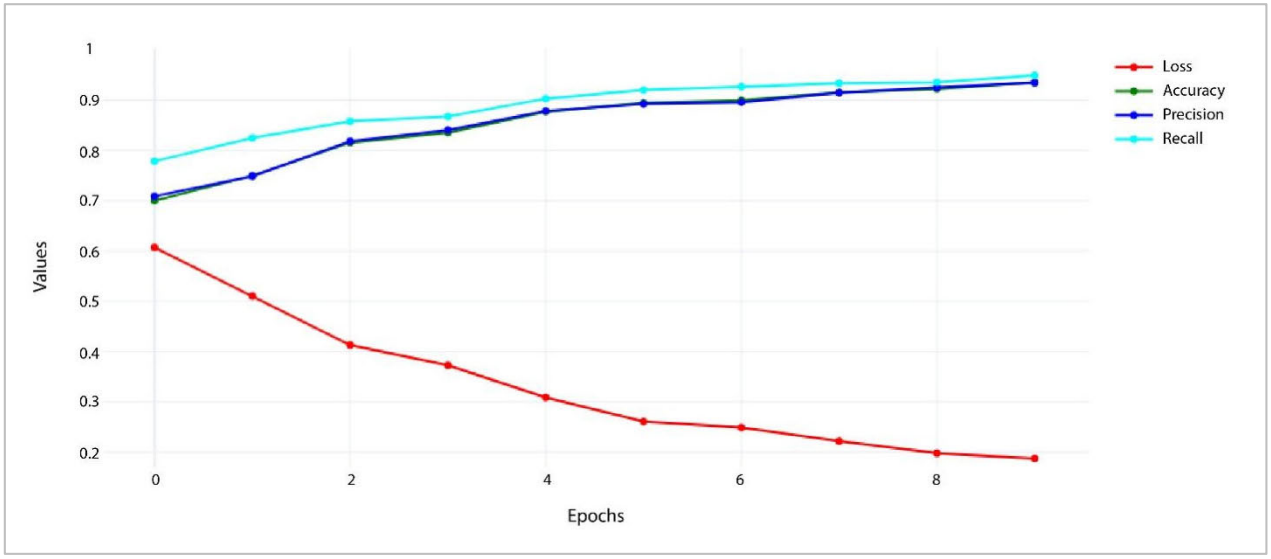

(a)

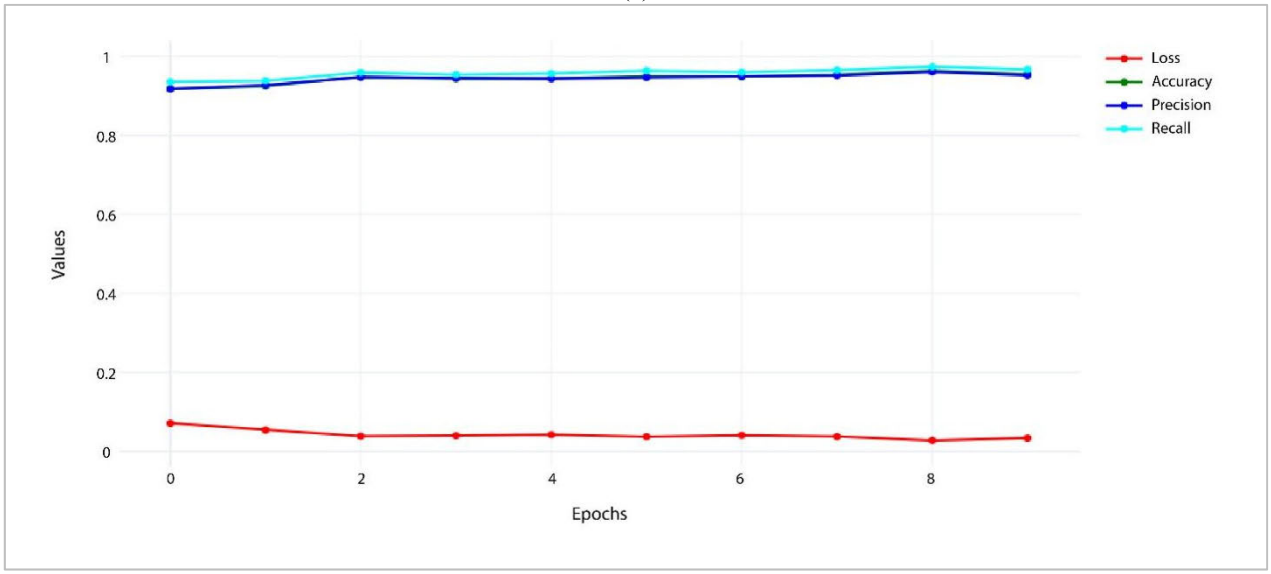

(b)

FIGURE 4. The performance of the model DenseNet201 makes use of (a) the binary_crossentropy loss function and (b) the BinaryFocalLoss loss function.

TABLE 6. Summarized fine-tuned parameters description of InceptionResNetV2's binary cross entropy.

Name	Description
Loss	binary_crossentropy
Optimizer	Adam
Learning Rate	0.001
epochs	10

With Adam serving as the optimizer and a 0.001 learning rate. According to Table 7, this was carried out. The epoch was determined to be 10. Figures 5(a) and (b) show how well the model performs when employing the binary cross-entropy loss function and the binary focal loss. Both of these loss functions were considered by the model.

TABLE 7. Summarized fine-tuned parameters description of InceptionResNetV2's binary focal loss.

Name	Description
Loss	BinaryFocalLoss
Gamma	2.0
Optimizer	Adam
Learning Rate	0.001
epochs	10

The performance of the model is shown in Figure 5, and the red color denotes the losses the model endured. It also uses the extent of a line's green coloring as a measure of

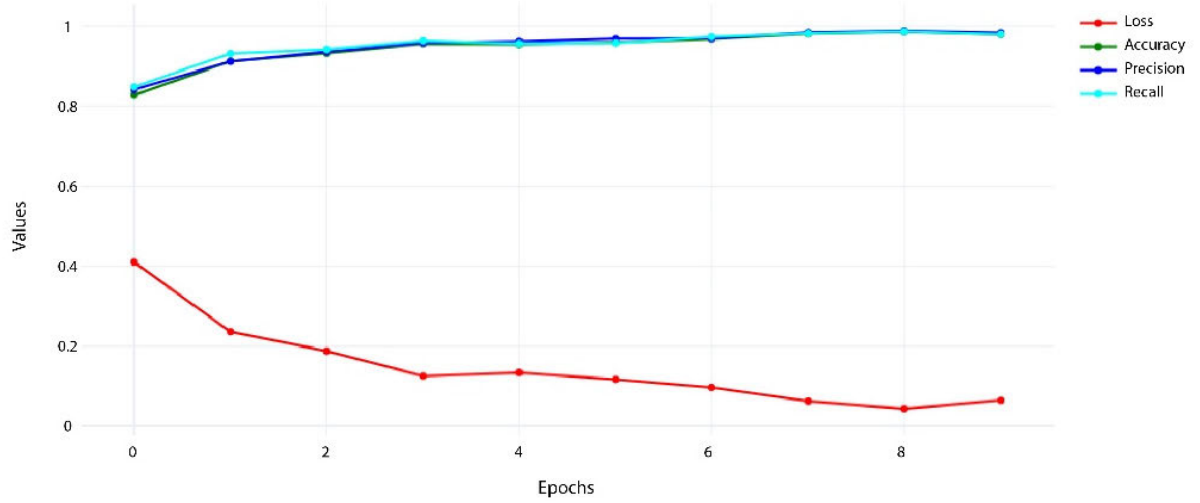

(a)

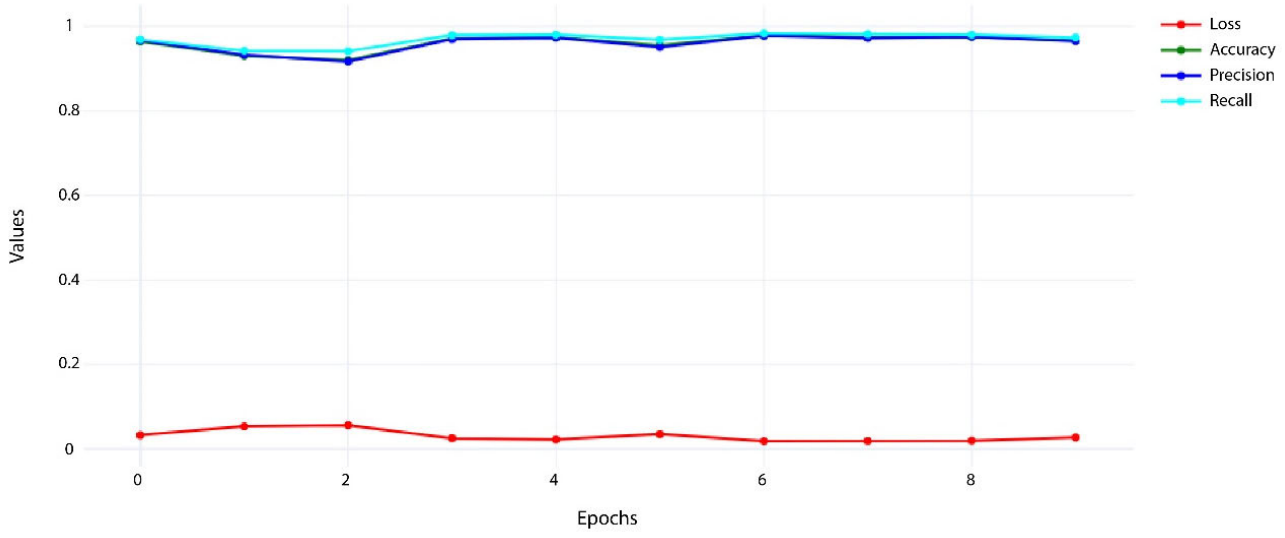

(b)

FIGURE 5. The performance of the model InceptionResNetV2 makes use of (a) the binary_crossentropy loss function and (b) the BinaryFocalLoss loss function.

the model's accuracy. Also demonstrated is the ability of the color blue to convey the level of precision that the model provides. Aside from that, the blue color represents the recall. The binary focal loss function's performance is greater than the binary cross entropy loss function when compared to each other. Given that, this is shown to be true. This results from the dataset's characteristic imbalance.

TABLE 8. Summarized fine-tuned parameters description of EfficientNetB7's binary cross entropy.

Name	Description
Loss	binary_crossentropy
Optimizer	Adam
Learning Rate	0.001
epochs	10

C. EfficientNetB7

EfficientNet is a technique for the building and scaling of convolutional neural networks [31]. This study's dataset was split into two categories, "Monkeypox" and "Others," using a modern pre-trained version of the EfficientNetB7 neural network. In Tables 8 and Table 9, respectively, the settings for binary cross entropy and binary focal loss are adjusted. The tables that follow include further information and specifics about these adjustments.

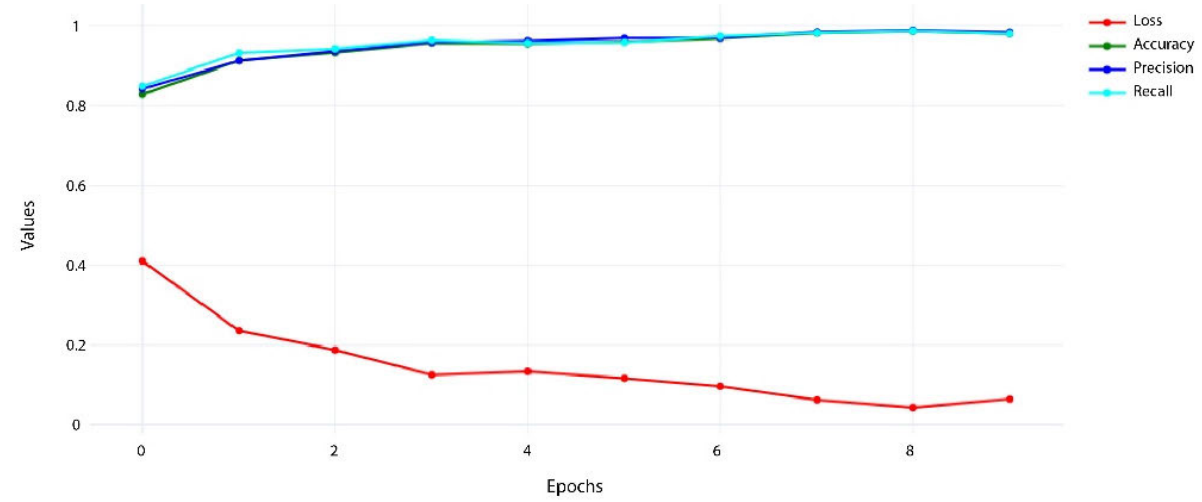

(a)

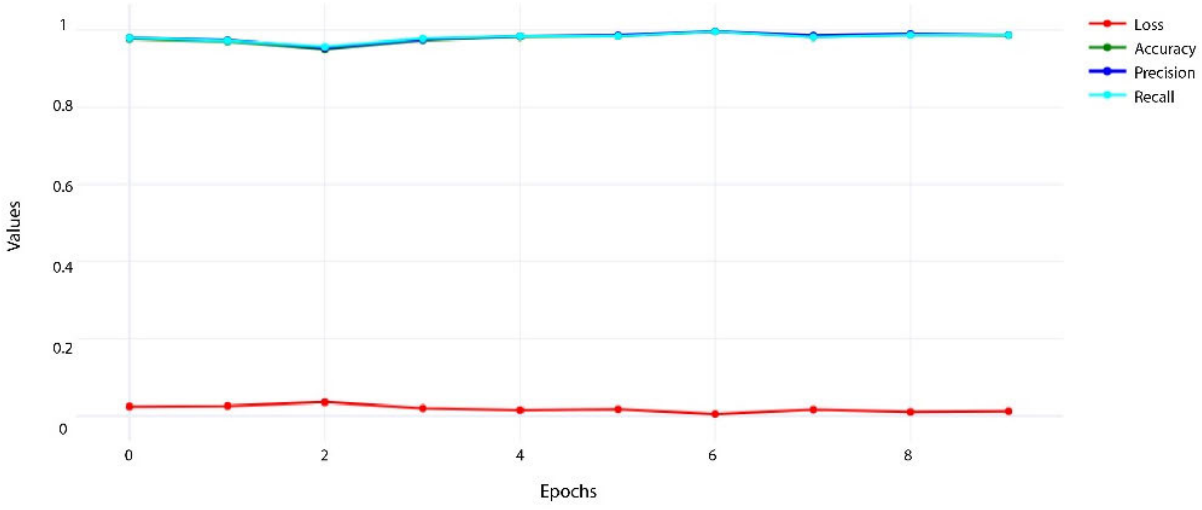

(b)

FIGURE 6. The performance of the model EfficientNetB7 makes use of (a) the binary_crossentropy loss function and (b) the BinaryFocalLoss loss function.

TABLE 9. Summarized fine-tuned parameters description of EfficientNetB7's binary focal loss.

Name	Description
Loss	BinaryFocalLoss
Gamma	2.0
Optimizer	Adam
Learning Rate	0.001
epochs	10

Table 8's information demonstrates that the loss function for the EfficientNetB7 model was binary cross-entropy. The learning rate was lowered to 0.001 and Adam was given the optimizer job. The epochs were represented by the number 10. The EfficientNetB7 model was then modified to include the BinaryFocalLoss loss function with gamma 2.0, Adam as the optimizer, and a learning rate of 0.001. Table 9 indicates that this was done. It was found that 10 was the epoch. The model performs well when using the binary cross-entropy loss function and the binary focal loss, as shown in Figures 6(a) and (b).

The model's performance is shown in Figure 6, and the red color indicates the losses of the model. The level of a line's green coloring is used to indicate the model's accuracy. The color blue expresses the precision level produced by the model is also illustrated. In addition, the recall is represented

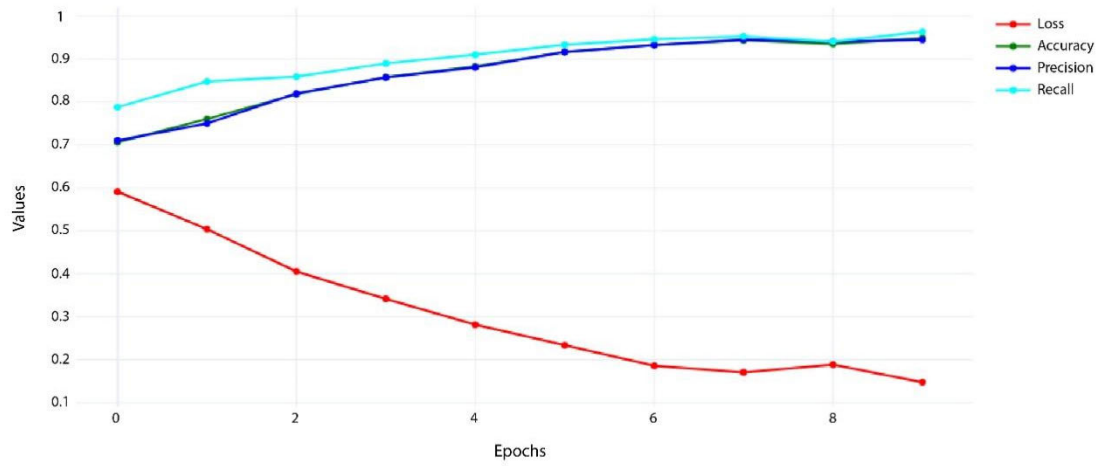

(a)

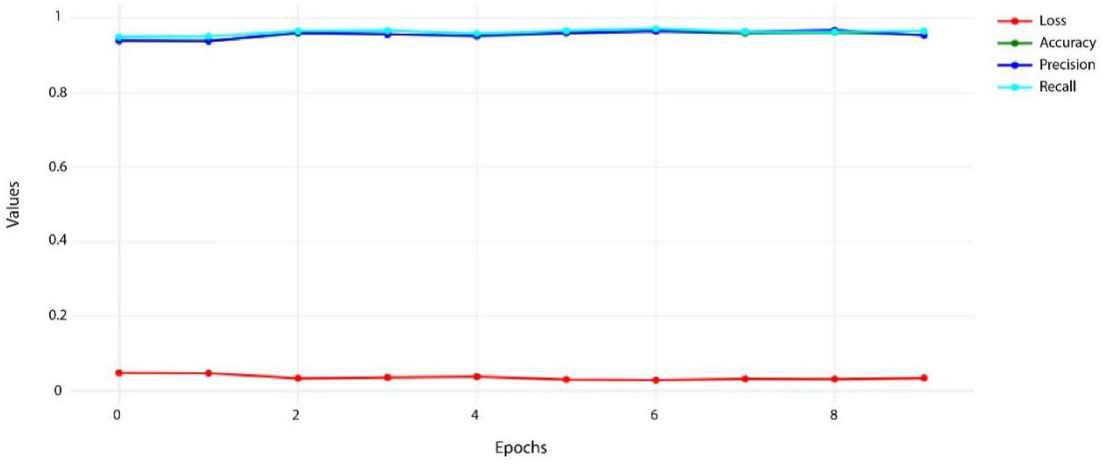

(b)

FIGURE 7. The performance of the model InceptionV3 makes use of (a) the binary_crossentropy loss function and (b) the BinaryFocalLoss loss function.

by the color cyan. The comparisons show that the binary cross entropy loss function outperforms the binary focal loss function. This is a result of the dataset's typical imbalance.

D. InceptionV3

Convolutional neural networks serve as the basic building block for the deep learning model InceptionV3, which is used to classify images. This model relies significantly on deep learning [32]. This study's dataset was divided into two categories: ''Monkeypox'' and ''Others,'' using a contemporary pre-trained version of the InceptionV3 neural network. The transfer learning technique was used to turn it into a feature extractor, and after that, two additional layers were added to InceptionV3 to improve it. To achieve the best level of performance feasible, changes have been made to the GlobalAveragePooling2D layer and the Dense layer's parameters. Two different loss matrices were used in the analytical procedure to account for the inconsistency that was found in the dataset. The two matrices that display these two matrices are the binary focal loss and the binary cross entropy. Brief explanations of the parameters' fine-tuning for binary cross entropy and binary focal loss are provided in Tables 10 and 11, respectively.

TABLE 10. Summarized fine-tuned parameters description of InceptionV3's binary cross entropy.

Name	Description
Loss	binary_crossentropy
Optimizer	Adam
Learning Rate	0.001
epochs	10

The loss function for the InceptionV3 model was initially set to binary cross-entropy, as can be shown in Table 10.

TABLE 11. Summarized fine-tuned parameters description of InceptionV3's binary focal loss.

Name	Description
Loss	BinaryFocalLoss
Gamma	2.0
Optimizer	Adam
Learning Rate	0.001
epochs	10

Adam was chosen to take on the role of the optimizer with a learning rate of 0.001. Epochs were configured to 10. Thereafter, in accordance with Table 11, the loss function for the InceptionV3 model was once more adjusted to BinaryFocalLoss with gamma 2.0, the optimizer Adam, and the learning rate 0.001. The value of an epoch was 10. The performance of the model while applying the binary cross-entropy loss function and the binaryFocalLoss loss function is shown in Figures 7(a) and (b), respectively.

Figure 7 shows the model's performance, with the color red representing the losses of the model. The accuracy of the model is determined by the degree to which a line in the graph is tinted green. The level of precision of the model is also shown to be represented by the color blue. Also, the model's recall, which cyan stands for. If the performance of the binary cross entropy loss function is compared to the performance of the binary focal loss function, the binary cross entropy loss function performs worse. This occurs as a result of the dataset's intrinsic imbalance.

E. ResNet50

The Resnet50 model, which makes use of deep learning, has already undergone training. There are a total of 50 layers in this convolutional neural network. The pre-trained network can classify images into a thousand different object categories [33]. Brief descriptions of the parameters for binary cross entropy and binary focal loss are given in Tables 12 and Table 13. The tables that follow provide further details and other information about these changes.

TABLE 12. Summarized fine-tuned parameters description of Resnet50's binary cross entropy.

Name	Description
Loss	binary_crossentropy
Optimizer	Adam
Learning Rate	0.001
epochs	10

Table 12's data reveals that the loss function for the ResNet50 model was binary cross-entropy. The optimizer job was given to Adam, and the learning rate was set to 0.001. The number 10 remained there throughout the ages. After that, Adam was used as the optimizer with a learning rate of 0.001 and BinaryFocalLoss with gamma 2.0 as the loss function for the ResNet50 model. Table 13 demonstrates that

TABLE 13. Summarized fine-tuned parameters description of Resnet50's binary focal loss.

Name	Description
Loss	BinaryFocalLoss
Gamma	2.0
Optimizer	Adam
Learning Rate	0.001
epochs	10

TABLE 14. Summarized fine-tuned parameters description of VGG16's binary cross entropy.

Name	Description
Loss	binary_crossentropy
Optimizer	Adam
Learning Rate	0.001
epochs	10

TABLE 15. Summarized fine-tuned parameters description of VGG16's binary focal loss.

Name	Description
Loss	BinaryFocalLoss
Gamma	2.0
Optimizer	Adam
Learning Rate	0.001
epochs	10

10 was selected as the epoch. Figures 8(a) and (b) show, respectively, how well the model performs when applied to the binary cross-entropy loss function and the binary focal loss. The model took both of these loss functions into account.

Figure 8 displays the model's performance, and red denotes the model's losses. The level of a line's green coloring is an indicator of the model's accuracy. Blue is used to show the level of precision that the model has achieved. In addition, the color cyan stands in for the recall. The binary cross entropy loss function works better than the binary focal loss function, as comparisons show. This is due to the usual imbalance in the dataset.

F. VGG16

A convolutional neural network with 16 layers is called VGG16. Transfer learning makes this straightforward to implement this technique [34]. The settings for binary cross entropy and binary focal loss are changed in Tables 14 and Table 15, respectively. The tables that follow provide further details and additional information about these revisions.

Table 14's data reveals that the VGG16 model's initial loss function was binary cross-entropy. Adam was designated as the optimizer, and the learning rate was set to 0.001. The epochs were set by the number 10. The BinaryFocalLoss loss function with gamma 2.0, Adam as the optimizer, and a learning rate of 0.001 were then added to the VGG16 model. The epoch was determined to be 10 as shown in Table 15.

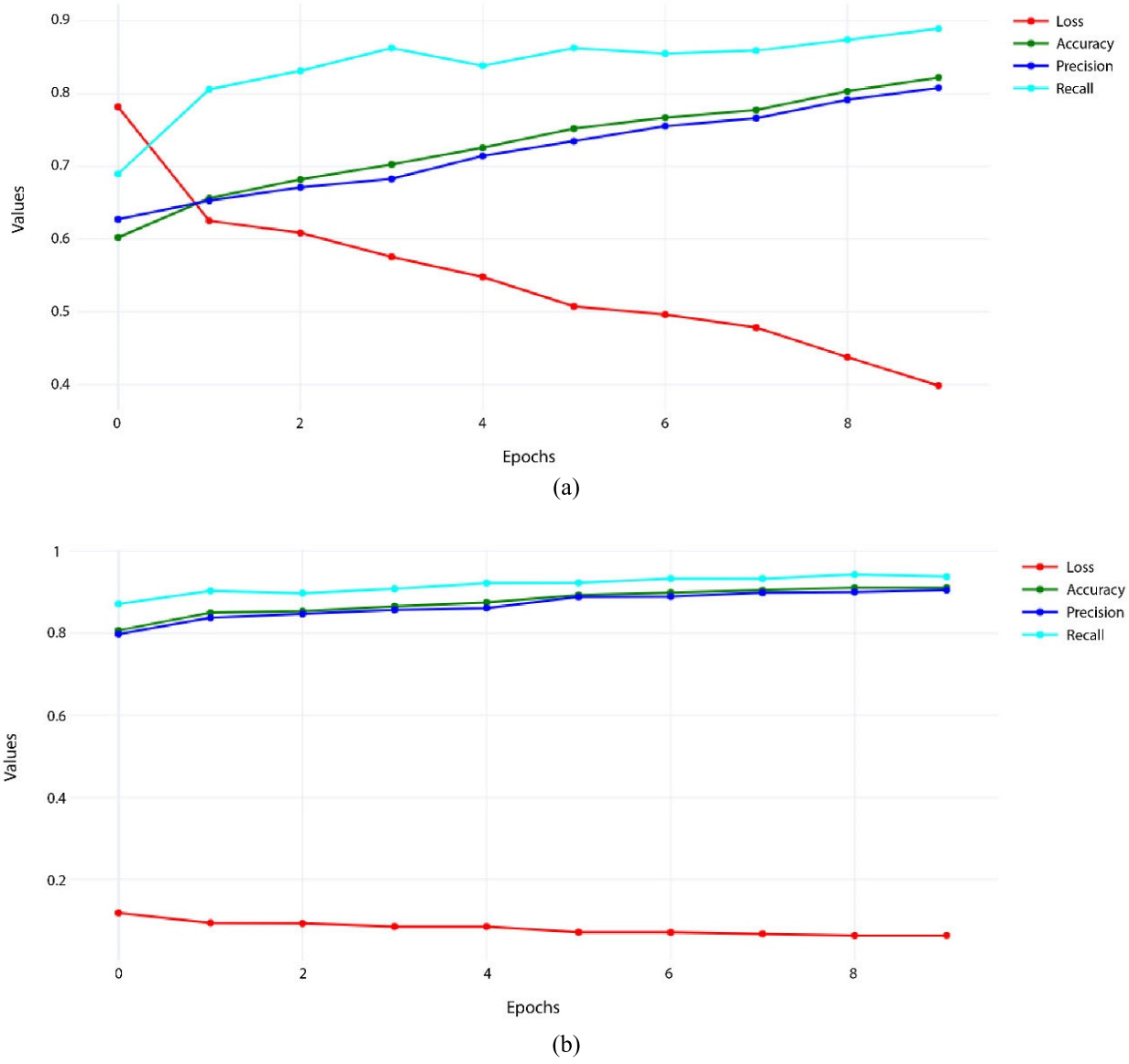

FIGURE 8. The performance of the model ResNet50 makes use of (a) the binary_crossentropy loss function and (b) the BinaryFocalLoss loss function.

According to Figures 9 (a) and (b), the model works well when the binary cross-entropy loss function and binary focal loss are used.

Figure 9 displays the model's performance, and red denotes the model's losses. The degree of a line's green coloring serves as a measure of the model's precision. Additionally, an illustration using the color blue to represent the model's level of precision is provided. In addition, the color cyan appears in the recall. The binary cross entropy loss function works better than the binary focal loss function, as shown by comparisons.

The effectiveness of those six models is going to be evaluated at this point to determine which one is the best. The four different matrices used to evaluate the effectiveness of those models are accuracy, precision, recall, and loss. Additionally, the model's execution time will be taken into account.

X. PERFORMANCE MATRICES

This study uses three widely used performance metrics: Precision, Recall, and Accuracy (1-3).

$$P = \frac{TP}{TP + FP} \tag{1}$$

$$R = \frac{TP}{TP + FN} \tag{2}$$

$$A = \frac{TP + TN}{TP + TN + FP + FN} \tag{3}$$

where, respectively, TP, TN, FP, FN, and $FPFN$ stand for true positive, true negative, false positive, and false negative.

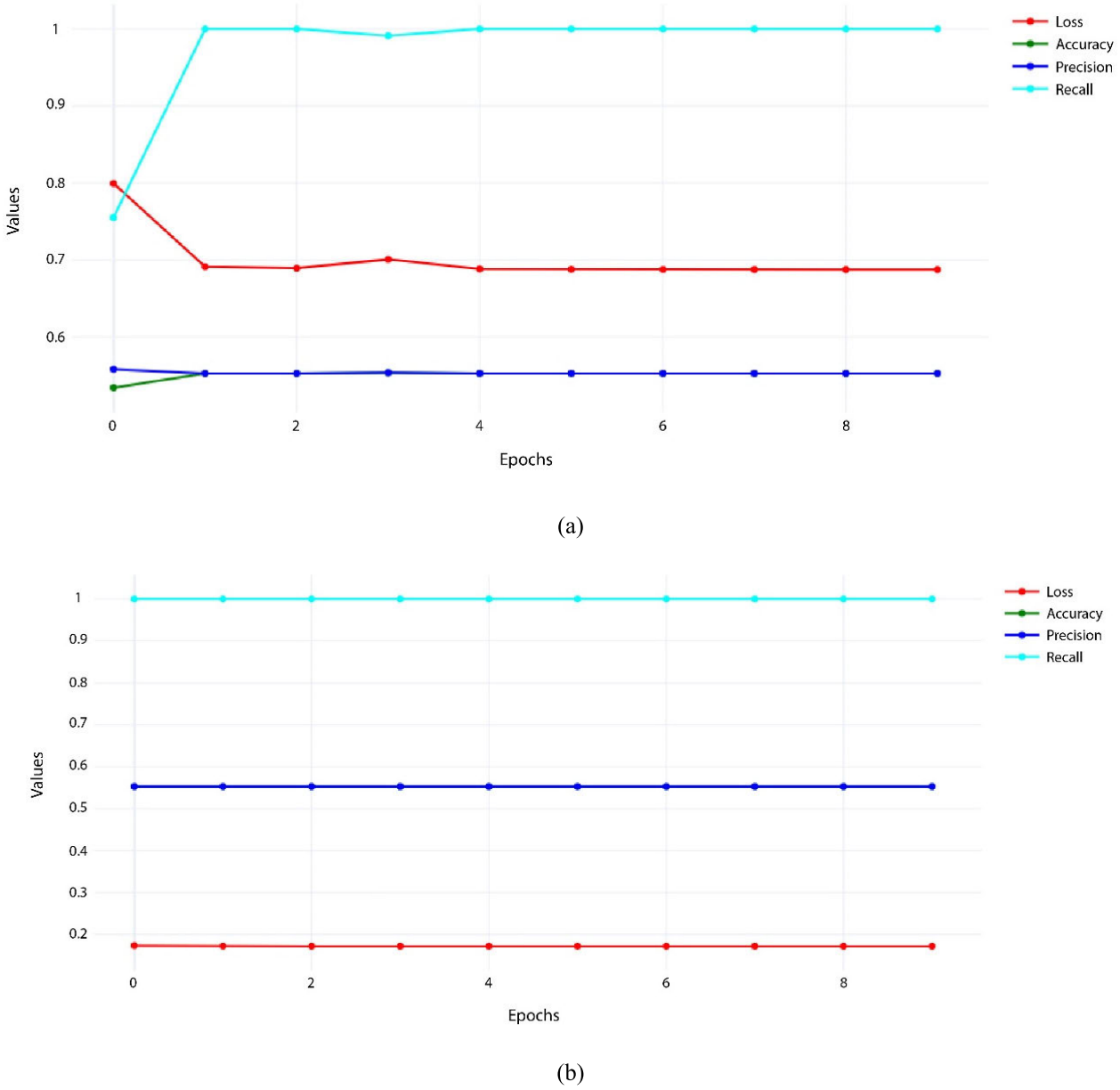

FIGURE 9. The performance of the model VGG16 makes use of (a) the binary_crossentropy loss function and (b) the BinaryFocalLoss loss function.

Similar to *P*, *R*, and *A*, *P*, *R*, and *A*, respectively, stand for Precision, Recall, and Accuracy [41].

XI. MODEL SELECTION

With the loss matrix set to the binary cross entropy, the DenseNet201 model's performance matrices achieved 92% accuracy, 92% precision, 93% recall, and 19% loss. And the model's execution took 7 minutes and 14 seconds. Additionally, 96% accuracy, 95% precision, 98% recall, and 9% loss were attained by the InceptionResNetV2 model. Also, it took 8 minutes and 49 seconds to execute the model. The EfficientNetB7 model achieved 94% accuracy, 94% precision, 96% recall, and 15% loss. The model's execution took 9 minutes and 45 seconds. The InceptionV3 model also achieved 99% accuracy, 99% precision, 98% recall, and 7% loss. The model's execution also took 6 minutes and 41 seconds. The ResNet50 model additionally achieved 83% accuracy, 81% precision, 89% recall, and 40% loss. The execution of the model took 8 minutes and 23 seconds. Lastly, The VGG16 model obtained 55% accuracy, 55% precision, 100% recall, and 68% loss. The model's execution took 6 minutes and 50 seconds. The summarized performance description of all six models is shown in Table 16.

TABLE 16. Summarized performance description of all models with loss matrix 'binary cross entropy'.

Model Name	Accuracy	Precision	Recall	Loss	Times (min/sec)
DenseNet201	92%	92%	93%	19%	7m 14s
InceptionResNetV2	96%	95%	98%	9%	8m 49s
EfficientNetB7	94%	94%	96%	15%	9m 45s
InceptionV3	**99%**	**99%**	98%	**7%**	**6m 41s**
ResNet50	83%	81%	89%	40%	8m 23s
VGG16	55%	55%	**100%**	68%	6m 50s

With the loss matrix set to the binary-focused loss, the performance matrices of the DenseNet201 model once more yielded 96% accuracy, 96% precision, 97% recall, and 4% loss. It took 7 minutes and 17 seconds to run the model. Also achieving 96% accuracy, 95% precision, 97% recall, and 2% loss was the InceptionResNetV2 model. Also, the execution of the model took 8 minutes and 13 seconds. The EfficientNetB7 model obtained 95% accuracy, 96% precision, 97% recall, and 5% loss. The model's execution took 9 minutes and 44 seconds. Additionally, the InceptionV3 model obtained 99% accuracy, 99% precision, 99% recall, and 0.3% loss. The model's execution also took 6 minutes and 40 seconds. The ResNet50 model also achieved 91% accuracy, 90% precision, 93% recall, and 7% loss. The model execution took 7 minutes and 2 seconds. Lastly, 55% accuracy, 55% precision, 100% recall, and 17% loss were attained with the VGG16 model. It took 6 minutes and 48 seconds to run the model. Table 17 displays a summary of each model's performance description.

TABLE 17. Summarized performance description of all models with loss matrix 'binary focal loss'.

Model Name	Accuracy	Precision	Recall	Loss	Times (min/sec)
DenseNet201	96%	96%	97%	4%	7m 17s
InceptionResNetV2	96%	95%	97%	2%	8m 13s
EfficientNetB7	95%	96%	97%	5%	9m 44s
InceptionV3	**99%**	**99%**	99%	**0.3%**	**6m 40s**
ResNet50	91%	90%	93%	7%	7m 2s
VGG16	55%	55%	**100%**	17%	6m 48s

According to Table 16 and Table 17, the InceptionV3 model outperforms the other six models, according to the comparison of the loss matrix's Binary Cross Entropy and Binary Focal Loss metrics. And when compared to these two loss matrices, Binary Cross Entropy and Binary Focal Loss, the performance of Binary Focal Loss are far superior. As a result, this work aims to develop a model by improving the InceptionV3 model's parameters.

XII. PROPOSED MODEL

The model that is being proposed in this research PoxNet22 is a fine-tuned version of the InceptionV3 model. Where The strategy of transfer learning was applied to turn it into a feature extractor, and after that, two additional layers were added to the model to improve it. Ultimately, the model was successful in performing its new function. Both the GlobalAveragePooling2D layer and the Dense layer's settings have been modified to achieve the maximum level of technically attainable performance. This has been done to accomplish the goal of achieving the highest level of performance. Figure 10 presents the model's underlying architectural framework.

As can be seen in figure 10, there are a total of six blocks, each of which is represented by a dotted rectangle. The first block comes after the input layer and includes a conv2D layer, a batch normalization layer, and an activation layer. The other block, which comes before the maxpooling2D layer, consists of one additional conv2D layer, batch normalization layer, and activation layer. This block comes before the maxpooling2D layer. In general, the max operation is used to pool sets of features in Max pooling, which results in fewer of those features remaining after the process. As a result, the model employs a max-pooling layer to reduce overfit. The line with dots indicates that there are three more blocks consisting of the same layers in between these two blocks. These blocks can be found between these two blocks.

Following that, a total of four further blocks are produced by the maxpooling2D layer. One layer for converting 2D to 1D, one for batch normalization, and one for activation make up a single block. Three levels of batch normalization, three layers of conv2D, and three layers of activation make up another block. Two conv2D layers, two batch normalization layers, and two activation layers are part of another block. Another one has a batch normalization layer, an average pooling 2D layer, a conv2D layer, and an activation layer. The average value for various feature map portions was calculated using the average pooling 2D layer to create a down-sampled feature map. The mixed0 layer is created by concatenating the output of these four blocks. Between the mixed0 layer and the mixed10 layer, nine additional blocks are identical to the previously mentioned ones. The dot-filled line serves as a visual cue to this.

Last but not least, to reduce the overall number of parameters in the model and avoid overfitting, one global average pooling layer has been inserted between the mixed10 layer and the output layer itself. There are 21,804,833 parameters in the model as a whole. In this case, the trainable parameters are 21,770,401, whereas the non-trainable parameters are 34,432.

The model is now in a state where it can effectively run the experiment. The following is a description of the next stage, which can be found in the result analysis section.

XIII. RESULT ANALYSIS

To extract the best possible performance level from the PoxNet22 model, the essential ablution study has been carried out on the dataset collected in the manner detailed below.

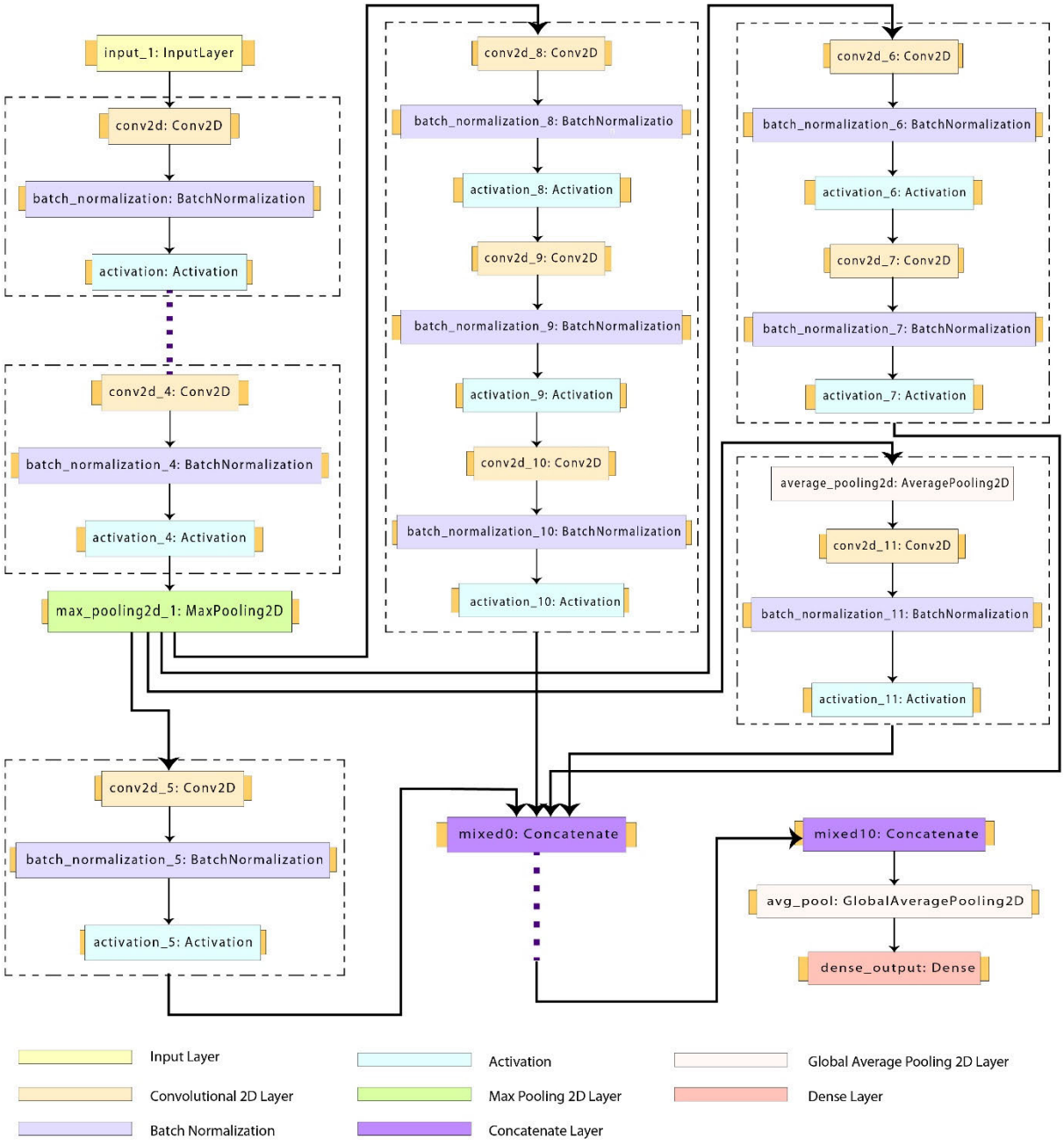

FIGURE 10. The architecture of the proposed model PoxNet22. Where the input layer is denoted by orange color, the convolution 2D layer is denoted by bottle green color, batch normalization is denoted by ash color, activation is denoted by purple color, max pooling 2D layer is denoted by green color, concatenate layer is denoted by blue color, global average pooling 2D layer is denoted by magenta color and dense layer the output layer is denoted red color.

A. ABLUTION STUDY

Both an SGD optimizer (also known as stochastic gradient descent) and an ADAM optimizer were utilized in the process of this study. There have been numerous shifts in the learning rate for both the values of 0.001 and 0.0001. In addition to that, the values 2.0 and 0.22 have been utilized for the gamma parameter. The number of epochs has been concurrently set to the values of 10 and 20 and 30. As a result, the model was executed twenty-four times using a variety of parameter combinations. In table 18, there can find a summary of the ablution study that was done with the PoxNet22 model.

According to the information presented in Table 18, the optimizer SGD epochs were 20 when the learning rate was 0.001, and the gamma value was 0.22. The SGD optimizer was able to get the best performance by these parameter attributes. On the other hand, when the learning rate was 0.0001, the gamma value was 0.22, and the number of epochs was 30 for the optimizer ADAM. And the ADAM optimizer

TABLE 18. The summarized description of ablution study of the Poxnet22 model.

Optimizer	Learning Rate	Gamma	epochs	Accuracy	Precision	Recall	Loss	Times (min/sec)
SGD	(0.001)	2.0	10	98%	98%	99%	4%	06m 56s
SGD	(0.001)	2.0	20	98%	98%	99%	3%	13m 37s
SGD	(0.001)	2.0	30	97%	96%	99%	1%	20m 22s
SGD	(0.0001)	2.0	10	66%	68%	72%	15%	06m 48s
SGD	(0.0001)	2.0	20	78%	78%	85%	11%	13m 11s
SGD	(0.0001)	2.0	30	87%	85%	93%	8%	19m 40s
SGD	(0.001)	0.22	10	98%	98%	99%	4%	06m 41s
SGD	**(0.001)**	**0.22**	**20**	**99%**	**99%**	**99%**	**0.01%**	**13m 04s**
SGD	(0.001)	0.22	30	99%	99%	99%	3%	19m 31s
SGD	(0.0001)	0.22	10	89%	85%	96%	29%	06m 39s
SGD	(0.0001)	0.22	20	92%	89%	97%	20%	13m 09s
SGD	(0.0001)	0.22	30	95%	93%	98%	12%	19m 30s
Adam	(0.001)	2.0	10	99%	99%	99%	0%	06m 40s
Adam	(0.001)	2.0	20	95%	92%	100%	3%	13m 17s
Adam	(0.001)	2.0	30	96%	99%	94%	2%	20m 08s
Adam	(0.0001)	2.0	10	99%	99%	100%	0%	06m 41s
Adam	(0.0001)	2.0	20	99%	99%	99%	0%	14m 21s
Adam	(0.0001)	2.0	30	100%	100%	100%	0.05%	20m 26s
Adam	(0.001)	0.22	10	99%	99%	99%	0%	07m 33s
Adam	(0.001)	0.22	20	99%	99%	100%	0%	13m 23s
Adam	(0.001)	0.22	30	98%	98%	98%	3%	19m 51s
Adam	(0.0001)	0.22	10	99%	99%	99%	0%	06m 39s
Adam	(0.0001)	0.22	20	99%	99%	99%	0%	13m 07s
Adam	**(0.0001)**	**0.22**	**30**	**100%**	**100%**	**100%**	**0%**	**19m 40s**

attained the best performance by these parameter attributes. Figures 11 and 12 depict the ideal results that the PoxNet22 model produced for the SGD optimizer and the ADAM optimizer, respectively.

As shown in figure 11 and figure 12, the performance of the PoxNet22 model achieved a recall rate of 99%, 99% accuracy, and 0.01% loss. It also achieved 99% precision. Which requires a total of 13 minutes and 4 seconds to carry out. Besides that, the performance of the model achieved a recall rate of 100 %, an accuracy of 100 %, a precision of 100 %, and a loss of 0%. This requires a total of 19 minutes and 40 seconds to carry out. The PoxNet22 has performed outstandingly with the ADAM optimizer compared to the SGD optimizer. Therefore, ADAM has been selected as the final optimizer for the PoxNet22 model. And learning rate is determined to be 0.0001. In addition to that, the gamma value determines 0.22. And it is determined that 30 epochs are necessary for the model to operate at its best.

The dataset has now been subjected to the PoxNet22 model, both with and without augmentation, in order to compare the outcomes. This can justify the significance of data augmentation by stating the following.

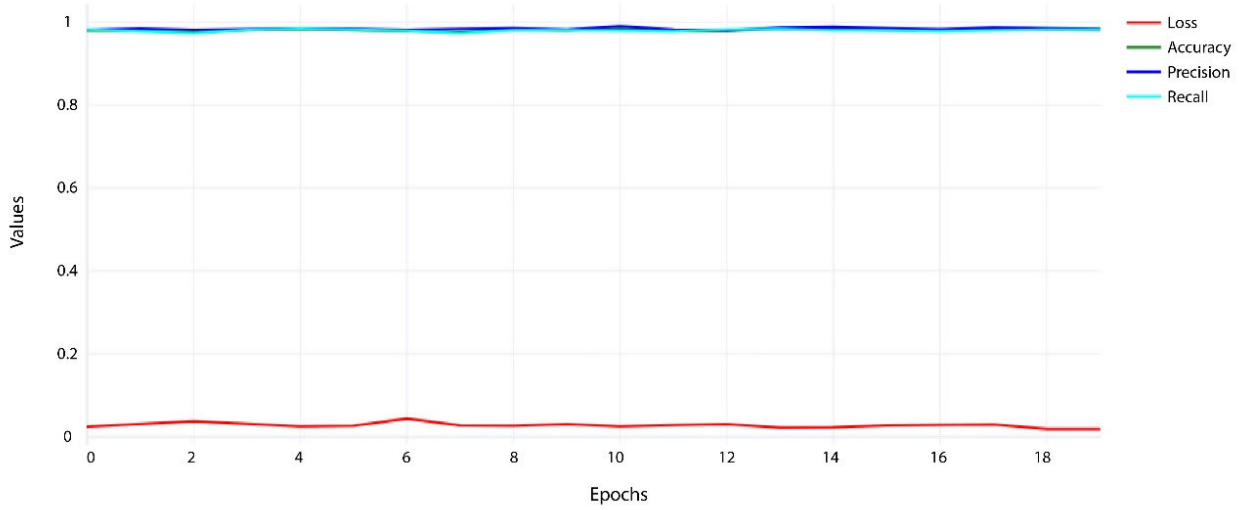

FIGURE 11. The optimal performance of the PoxNet22 with SGD optimizer.

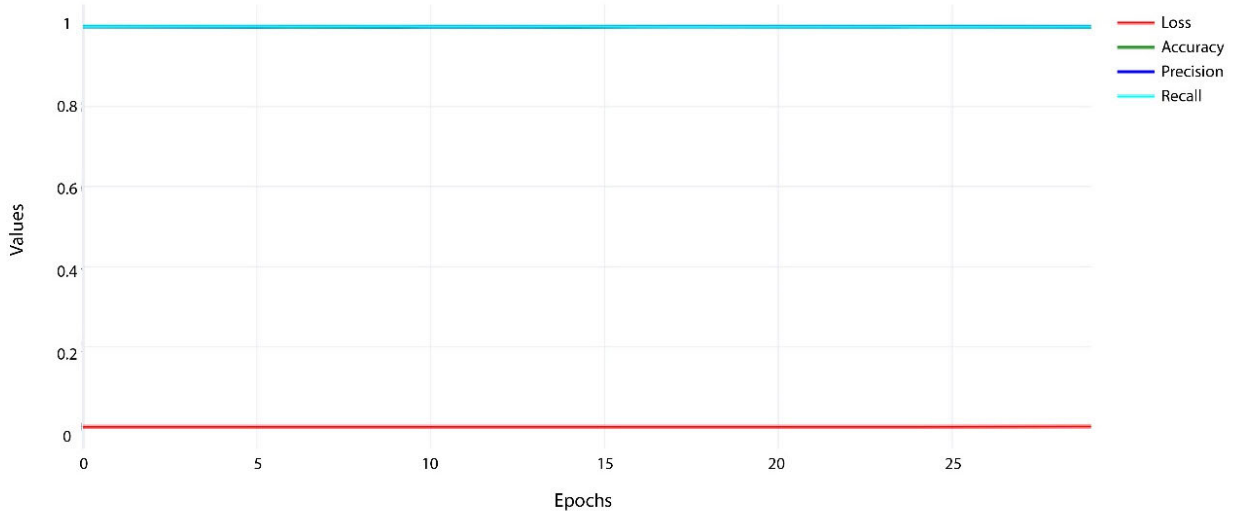

FIGURE 12. The optimal performance of the PoxNet22 with ADAM optimizer.

TABLE 19. The summarized description of the PoxNet22 model's performance with and without data augmentation.

Augmentation	Optimizer	Learning Rate	Gamma	epochs	Accuracy	Precision	Recall	Loss	Times (min/sec)
Without Augmentation	Adam	(0.0001)	0.22	30	97%	97%	98%	4%	20m 50s
With Augmentation	Adam	(0.0001)	0.22	30	100%	100%	100%	0%	19m 40s

B. THE BENEFIT OF DATA AUGMENTATION

The data set does not have sufficient images, as was mentioned before in the section on data augmentation. As a result, data augmentation was carried out to reduce the possibility of the model overfitting issue occurring.

The PoxNet22 model without any data augmentation, using the optimizer ADAM, learning rate 0.0001, gamma value 0.22, and number of epochs 30. The accuracy of the model was 97%, its precision was also 97%, its recall was 98%, and its loss was 4%. Which must be carried out in a

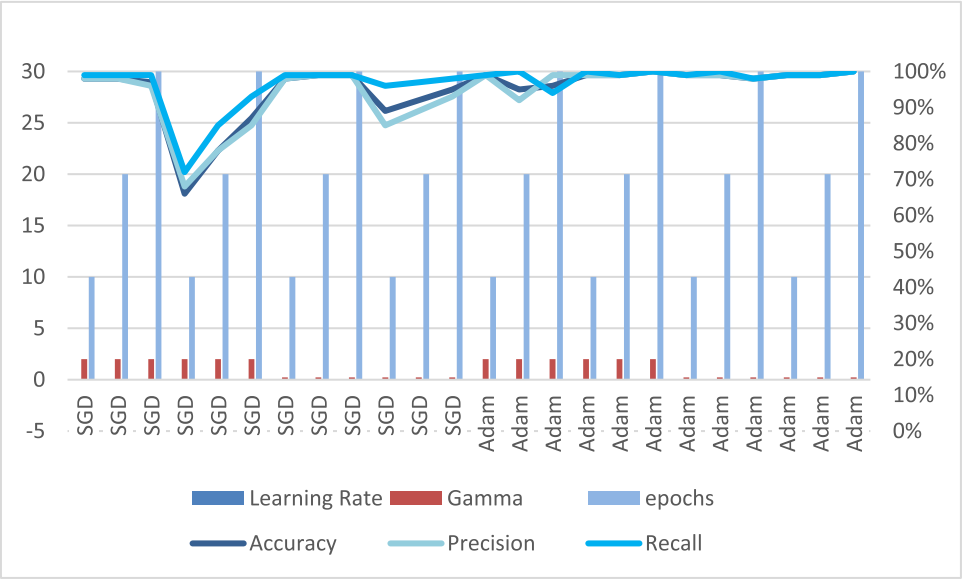

FIGURE 13. The optimal performance of the PoxNet22 with fine-tuned parameters.

TABLE 20. The summarized comparison of the PoxNet22 model's performance with the state of the arts.

Method	Description	Dataset	Accuracy	Precision	Recall	Findings
Abdelhamid et al., [13]	SCBER+NN	Monkeypox Skin Images Dataset (MSID)	98.8%	-	-	Monkeypox classification
Sitaula et al., [14]	Ensemble approach (Xception & DenseNet-169)	Monkeypox image dataset (MID)	87.13%	85.44%	85.47%	Monkeypox classification
Ali et al., [2]	ResNet50	Monkeypox Skin Lesion Dataset (MSLD)	82.96%	87%	83%	Monkeypox classification
	VGG16		81.48%	85%	81%	
	InceptionV3		74.07%	74%	81%	
	Ensemble trio (ResNet50, VGG16 & InceptionV3)		79.26%	84%	79%	
Proposed	**PoxNet22**	**(MSLD)** [15]	**100%**	**100%**	**100%**	**Monkeypox classification**

total of 20 minutes and 50 seconds. Since, after having its data enhanced, the model was able to achieve 100% accuracy, 100% precision, 100% recall, and 0% loss. The parameter settings in this instance were unchanged from the previous ones. An overview of the PoxNet22 model's performance with and without the data augmentation described in table 19 is provided below.

Compared to the performance of the model without data augmentation, it is abundantly clear that the performance of the PoxNet22 model is much improved when provided with augmented data.

XIV. DISCUSSION

The optimizer for the PoxNet22 model used 20 SGD epochs, 0.001 learning rate, and 0.22 gamma as its parameters. This parameter contributes to the optimal performance of the SGD optimizer. The optimizer ADAM had 30 epochs under its belt with a gamma value of 0.22 at a learning rate of 0.0001. The ADAM optimizer functioned more effectively because of these parameter properties. PoxNet22 has a 99% recall rate, a 99% accuracy rating, and a 0.01% loss rate. It was correct 99% of the time. All told, there are 13 minutes and 4 seconds. In addition, the model exhibits perfect recall, accuracy, precision, and loss. It takes 19 minutes and 40 seconds for this. Performance-wise, the ADAM optimizer in PoxNet22 outperformed the SGD optimizer. As a result, ADAM serves as PoxNet22's ultimate optimizer. The learning rate is 0.0001 percent. With a value of 0.22 for gamma when run with 30 epochs, the model functions most effectively. The optimal performance of the PoxNet22 with fine-tuned parameters have shown in figure 13.

Figure 13 provides a detailed illustration of how the parameters have been adjusted to get the greatest possible performance. Where the color blue stands for a particular parameter such as the learning rate. The color orange is used to symbolize gamma. Epochs are denoted by shades of

ash. In addition, the color navy blue is used in performance matrices to denote accuracy. The color light blue denotes preciseness. The color neon blue denotes recall.

XV. COMPARING WITH EXITING WORK

Combining the Al-Biruni Earth radius optimization and sine cosine methods, Abdelhamid et al. [13] devised the SCBER optimization algorithm. The algorithms are evaluated using a public dataset. where categorization accuracy was on average 98.8%. To identify monkeypox using a public dataset, Sitaula et al. [14] suggested an ensemble technique (Xception & DenseNet-169). They were 87.13 percent accurate. Ali et al. [15] used pictures of measles, chickenpox, and monkeypox lesions from the ''Monkeypox Skin Lesion Dataset (MSLD)''. Then, the monkeypox is categorized using trained deep learning models like VGG-16, ResNet50, and InceptionV3. Three different models were built. Where the accuracy of the trio ensemble system is 79.26%, that of VGG16 is 81.48%, and that of ResNet50 is 82.96%. In contrast, the PoxNet22 has been used to identify monkey pox illnesses using the Monkeypox Skin Lesion Dataset (MSLD) [15] data set. And outperform all of these state-of-the-art works with 100 percent accuracy. The performance of the PoxNet22 model in comparison to the state of the art is reported in Table 20.

XVI. CONCLUSION

In this study, the dataset comprising monkeypox skin lesions was preprocessed, enhancing the photos' quality. And also executed the data augmentation procedure to lessen the probability of the model overfitting. Following that, we utilized a total of six distinct models on the dataset. We compared the results of those models to find the one that gave us the greatest results. According to the performance matrices, the PoxNet22 achieved the best possible performance, an accuracy value of 100%, a recall value of 100%, and a precision value of 100%. We can speak to the astonishing accuracy level employed in classifying monkeypox skin lesions. The paradigm that is outlined in this study offers both something new and something beneficial to clinical physicians. The lack of availability of high-quality images of monkeypox skin lesions as well as databases of greater sizes was the most significant constraint of our work. However, to optimize a model to its best potential, one must first have access to a dataset of high quality. In the future, we are going to carry on with our investigation into the existing issues.

ACKNOWLEDGMENT

The authors would like to acknowledge the Princess Nourah bint Abdulrahman University Researchers Supporting Project number (PNURSP2023R66), Princess Nourah bint Abdulrahman University, Riyadh, Saudi Arabia.

REFERENCES

[1] J. G. Rizk, G. Lippi, B. M. Henry, D. N. Forthal, and Y. Rizk, ''Prevention and treatment of monkeypox,'' *Drugs*, vol. 82, no. 9, pp. 957–963, Jun. 2022, doi: 10.1007/s40265-022-01742-y.

[2] F. S. Minhaj et al., ''Monkeypox outbreak—Nine states, May 2022,'' *Morbidity Mortality Weekly Rep.*, vol. 71, no. 23, pp. 764–769, Jun. 2022, doi: 10.15585/mmwr.mm7123e1.

[3] F.-M. Lum, A. Torres-Ruesta, M. Z. Tay, R. T. P. Lin, D. C. Lye, L. Rénia, and L. F. P. Ng, ''Monkeypox: Disease epidemiology, host immunity and clinical interventions,'' *Nature Rev. Immunol.*, vol. 22, no. 10, pp. 597–613, Oct. 2022, doi: 10.1038/s41577-022-00775-4.

[4] A. Sherwat, J. T. Brooks, D. Birnkrant, and P. Kim, ''Tecovirimat and the treatment of monkeypox—Past, present, and future considerations,'' *New England J. Med.*, vol. 387, no. 7, pp. 579–581, Aug. 2022, doi: 10.1056/NEJMp2210125.

[5] V. Ravi, H. Narasimhan, C. Chakraborty, and T. D. Pham, ''Deep learning-based meta-classifier approach for COVID-19 classification using CT scan and chest X-ray images,'' *Multimedia Syst.*, vol. 28, no. 4, pp. 1401–1415, Aug. 2022, doi: 10.1007/s00530-021-00826-1.

[6] Ç. Oğuz and M. Yağanoğlu, ''Detection of COVID-19 using deep learning techniques and classification methods,'' *Inf. Process. Manage.*, vol. 59, no. 5, Sep. 2022, Art. no. 103025, doi: 10.1016/j.ipm.2022.103025.

[7] N. Ullah, J. A. Khan, S. Almakdi, M. S. Khan, M. Alshehri, D. Alboaneen, and A. Raza, ''A novel CovidDetNet deep learning model for effective COVID-19 infection detection using chest radiograph images,'' *Appl. Sci.*, vol. 12, no. 12, p. 6269, Jun. 2022, doi: 10.3390/app12126269.

[8] A. Bhattacharyya, D. Bhaik, S. Kumar, P. Thakur, R. Sharma, and R. B. Pachori, ''A deep learning based approach for automatic detection of COVID-19 cases using chest X-ray images,'' *Biomed. Signal Process. Control*, vol. 71, Jan. 2022, Art. no. 103182, doi: 10.1016/j.bspc.2021.103182.

[9] M. R. Hassan, M. F. Islam, M. Z. Uddin, G. Ghoshal, M. M. Hassan, S. Huda, and G. Fortino, ''Prostate cancer classification from ultrasound and MRI images using deep learning based explainable artificial intelligence,'' *Future Gener. Comput. Syst.*, vol. 127, pp. 462–472, Feb. 2022, doi: 10.1016/j.future.2021.09.030.

[10] K. Jabeen, M. A. Khan, M. Alhaisoni, U. Tariq, Y.-D. Zhang, A. Hamza, A. Mickus, and R. Damaševičius, ''Breast cancer classification from ultrasound images using probability-based optimal deep learning feature fusion,'' *Sensors*, vol. 22, no. 3, p. 807, Jan. 2022, doi: 10.3390/s22030807.

[11] K. C. Figueroa et al., ''Interpretable deep learning approach for oral cancer classification using guided attention inference network,'' *J. Biomed. Opt.*, vol. 27, no. 1, Jan. 2022, Art. no. 015001, doi: 10.1117/1.JBO.27.1.015001.

[12] K. Rezaee, G. Jeon, M. R. Khosravi, H. H. Attar, and A. Sabzevari, ''Deep learning-based microarray cancer classification and ensemble gene selection approach,'' *IET Syst. Biol.*, vol. 16, nos. 3–4, pp. 120–131, May 2022, doi: 10.1049/syb2.12044.

[13] A. A. Abdelhamid, E.-S.-M. El-Kenawy, N. Khodadadi, S. Mirjalili, D. S. Khafaga, A. H. Alharbi, A. Ibrahim, M. M. Eid, and M. Saber, ''Classification of monkeypox images based on transfer learning and the Al-Biruni Earth radius optimization algorithm,'' *Mathematics*, vol. 10, no. 19, p. 3614, Oct. 2022, doi: 10.3390/math10193614.

[14] C. Sitaula and T. B. Shahi, ''Monkeypox virus detection using pre-trained deep learning-based approaches,'' *J. Med. Syst.*, vol. 46, no. 11, p. 78, Oct. 2022, doi: 10.1007/s10916-022-01868-2.

[15] S. N. Ali, M. T. Ahmed, J. Paul, T. Jahan, S. M. S. Sani, N. Noor, and T. Hasan, ''Monkeypox skin lesion detection using deep learning models: A feasibility study,'' Jul. 2022, *arXiv:2207.03342*.

[16] M. Bhandari, T. B. Shahi, B. Siku, and A. Neupane, ''Explanatory classification of CXR images into COVID-19, pneumonia and tuberculosis using deep learning and XAI,'' *Comput. Biol. Med.*, vol. 150, Nov. 2022, Art. no. 106156, doi: 10.1016/j.compbiomed.2022.106156.

[17] M. Loey, S. El-Sappagh, and S. Mirjalili, ''Bayesian-based optimized deep learning model to detect COVID-19 patients using chest X-ray image data,'' *Comput. Biol. Med.*, vol. 142, Mar. 2022, Art. no. 105213, doi: 10.1016/j.compbiomed.2022.105213.

[18] E. Khan, M. Z. U. Rehman, F. Ahmed, F. A. Alfouzan, N. M. Alzahrani, and J. Ahmad, ''Chest X-ray classification for the detection of COVID-19 using deep learning techniques,'' *Sensors*, vol. 22, no. 3, p. 1211, Feb. 2022, doi: 10.3390/s22031211.

[19] A. H. Barshooi and A. Amirkhani, ''A novel data augmentation based on Gabor filter and convolutional deep learning for improving the classification of COVID-19 chest X-ray images,'' *Biomed. Signal Process. Control*, vol. 72, Feb. 2022, Art. no. 103326, doi: 10.1016/j.bspc.2021.103326.

[20] S. V. Kogilavani, J. Prabhu, R. Sandhiya, M. S. Kumar, U. Subramaniam, A. Karthick, M. Muhibbullah, and S. B. S. Imam, "COVID-19 detection based on lung CT scan using deep learning techniques," *Comput. Math. Methods Med.*, vol. 2022, pp. 1–13, Feb. 2022, doi: 10.1155/2022/7672196.

[21] K. Purohit, A. Kesarwani, D. R. Kisku, and M. Dalui, "COVID-19 detection on chest X-ray and CT scan images using multi-image augmented deep learning model," in *Proc. 7th Int. Conf. Math. Comput.*, Singapore, 2022, pp. 395–413, doi: 10.1007/978-981-16-6890-6_30.

[22] C. Ieracitano, N. Mammone, M. Versaci, G. Varone, A.-R. Ali, A. Armentano, G. Calabrese, A. Ferrarelli, L. Turano, C. Tebala, Z. Hussain, Z. Sheikh, A. Sheikh, G. Sceni, A. Hussain, and F. C. Morabito, "A fuzzy-enhanced deep learning approach for early detection of COVID-19 pneumonia from portable chest X-ray images," *Neurocomputing*, vol. 481, pp. 202–215, Apr. 2022, doi: 10.1016/j.neucom.2022.01.055.

[23] G. Latif, G. Ben Brahim, D. N. F. A. Iskandar, A. Bashar, and J. Alghazo, "Glioma tumors' classification using deep-neural-network-based features with SVM classifier," *Diagnostics*, vol. 12, no. 4, p. 1018, Apr. 2022, doi: 10.3390/diagnostics12041018.

[24] S. Rinesh, K. Maheswari, B. Arthi, P. Sherubha, A. Vijay, S. Sridhar, T. Rajendran, and Y. A. Waji, "Investigations on brain tumor classification using hybrid machine learning algorithms," *J. Healthcare Eng.*, vol. 2022, pp. 1–9, Feb. 2022, doi: 10.1155/2022/2761847.

[25] U. Zahid, I. Ashraf, M. A. Khan, M. Alhaisoni, K. M. Yahya, H. S. Hussein, and H. Alshazly, "BrainNet: Optimal deep learning feature fusion for brain tumor classification," *Comput. Intell. Neurosci.*, vol. 2022, pp. 1–13, Aug. 2022, doi: 10.1155/2022/1465173.

[26] K. Wei, T. Li, F. Huang, J. Chen, and Z. He, "Cancer classification with data augmentation based on generative adversarial networks," *Frontiers Comput. Sci.*, vol. 16, no. 2, Sep. 2021, Art. no. 162601, doi: 10.1007/s11704-020-0025-x.

[27] T. R. Mahesh, V. V. Kumar, V. Vivek, K. M. K. Raghunath, and G. S. Madhuri, "Early predictive model for breast cancer classification using blended ensemble learning," *Int. J. Syst. Assurance Eng. Manage.*, vol. 3, pp. 1–10, Jun. 2022, doi: 10.1007/s13198-022-01696-0.

[28] R. Kaur, H. GholamHosseini, R. Sinha, and M. Lindén, "Melanoma classification using a novel deep convolutional neural network with dermoscopic images," *Sensors*, vol. 22, no. 3, p. 1134, Feb. 2022, doi: 10.3390/s22031134.

[29] K. V. Hong, T. T. Minh, H. L. Duc, N. T. Nhat, and H. L. Hoang, "104 fruits classification using transfer learning and DenseNet201 fine-tuning," in *Complex, Intelligent and Software Intensive Systems*. Cham, Switzerland: Springer, 2022, pp. 160–170, doi: 10.1007/978-3-031-08812-4_16.

[30] N. Ullah, J. A. Khan, M. S. Khan, W. Khan, I. Hassan, M. Obayya, N. Negm, and A. S. Salama, "An effective approach to detect and identify brain tumors using transfer learning," *Appl. Sci.*, vol. 12, no. 11, p. 5645, Jun. 2022, doi: 10.3390/app12115645.

[31] D. Attota, D. N. Tadikonda, S. Pethe, and M. A. A. H. Khan, "An ensembled method for diabetic retinopathy classification using transfer learning," in *Proc. IEEE 46th Annu. Comput., Softw., Appl. Conf. (COMPSAC)*, Jun. 2022, pp. 1444–1449, doi: 10.1109/COMPSAC54236.2022.00229.

[32] P. Młodzianowski, "Weather classification with transfer learning—InceptionV3, MobileNetV2 and ResNet50," in *Digital Interaction and Machine Intelligence*. Cham, Switzerland: Springer, 2022, pp. 3–11, doi: 10.1007/978-3-031-11432-8_1.

[33] X. Zhao, K. Li, Y. Li, J. Ma, and L. Zhang, "Identification method of vegetable diseases based on transfer learning and attention mechanism," *Comput. Electron. Agricult.*, vol. 193, Feb. 2022, Art. no. 106703, doi: 10.1016/j.compag.2022.106703.

[34] D. Purkayastha and D. Malathi, "Leveraging transfer learning for effective recognition of emotions from images: A review," in *Cyber Security, Privacy and Networking*. Singapore: Springer, 2022, pp. 13–24, doi: 10.1007/978-981-16-8664-1_2.

[35] U. K. Lilhore, S. Simaiya, A. Kaur, D. Prasad, M. Khurana, D. K. Verma, and A. Hassan, "Impact of deep learning and machine learning in industry 4.0: Impact of deep learning," in *Cyber-Physical, IoT, and Autonomous Systems in Industry 4.0*. Boca Raton, FL, USA: CRC Press, 2021, pp. 179–197.

[36] C. Kaushal, D. Koundal, and A. Singla, "Comparative analysis of segmentation techniques using histopathological images of breast cancer," in *Proc. 3rd Int. Conf. Comput. Methodol. Commun. (ICCMC)*, Mar. 2019, pp. 261–266.

[37] A. Kaur, M. Khurana, P. Kaur, and M. Kaur, "Classification and analysis of water quality using machine learning algorithms," in *Proc. Int. Conf. Commun., Circuits, Syst.* Singapore: Springer, 2021, pp. 389–398.

[38] C. Kaushal, S. Bhat, D. Koundal, and A. Singla, "Recent trends in computer assisted diagnosis (CAD) system for breast cancer diagnosis using histopathological images," *IRBM*, vol. 40, no. 4, pp. 211–227, Aug. 2019.

[39] D. U. Ozsahin, M. T. Mustapha, B. Uzun, B. Duwa, and I. Ozsahin, "Computer-aided detection and classification of monkeypox and chickenpox lesion in human subjects using deep learning framework," *Diagnostics*, vol. 13, no. 2, p. 292, Jan. 2023, doi: 10.3390/diagnostics13020292.

[40] M. Altun, H. Gürüler, O. Özkaraca, F. Khan, J. Khan, and Y. Lee, "Monkeypox detection using CNN with transfer learning," *Sensors*, vol. 23, no. 4, p. 1783, Feb. 2023, doi: 10.3390/s23041783.

[41] D. Powers, "Evaluation: From precision, recall, and F-factor to ROC, informedness, markedness & correlation," *Mach. Learn. Technol.*, vol. 2, pp. 1–19, Jan. 2008.

FARHANA YASMIN received the B.Sc. degree from the Department of Computer Science and Engineering, Eastern University, Bangladesh. She is currently pursuing the Master of Science degree in computer applications and technology with Changzhou University, China. She is also an expert in computer vision, biomedical engineering, and data science, all of which are branches of artificial intelligence (AI). She works with scientists from all around the world to broaden her horizons and increase the depth of her expertise. Her research interests include predictive analysis and the development of expert systems.

MD. MEHEDI HASSAN (Member, IEEE) is currently pursuing the Master of Science (M.Sc.) degree in computer science and engineering with Khulna University, Khulna, Bangladesh. He is the Founder and the CEO of The Virtual BD IT Firm and VRD Research Laboratory, Bangladesh. He is also studying important human diseases, such as oncology, cancer, and hepatitis, as well as human behavior analysis. He is skilled in association rule mining, predictive analysis, machine learning, biomedical engineering, and expert systems. As a young researcher, he has published 22 articles in various international top journals and conferences. His research interests include biomedical and data science.

MAHADE HASAN received the Bachelor of Science degree in computer science and engineering from Eastern University, Bangladesh. He is currently pursuing the Master of Science degree in computer applications and technology with Changzhou University, China. He is an expert in all three of the artificial intelligence subfields of computer vision, image processing, and data analysis. He has written substantially on both subjects. His research interests include expert system design and image analysis.

SADIKA ZAMAN is currently pursuing the bachelor's degree in computer science and engineering with North Western University, Khulna, Bangladesh. She is also working on solving social problems. As a young researcher, she has six publications in international top journals and conferences. Her research interest includes biomedical engineering.

CHETNA KAUSHAL received the B.Tech. degree in information technology (IT) from Punjab Technical University and the M.Tech. degree in computer science and engineering (CSE) from DAV University, Punjab. She is currently pursuing the Ph.D. degree in CSE with Chitkara University, Punjab. She is working as an Assistant Professor with Chitkara University. Her areas of expertise are machine learning, soft computing, pattern recognition, image processing, and artificial intelligence. She has a total of nine years of experience in research, training, and academics. She has published several research papers in various international/national journals, books, and conferences. She has filed more than 20 international and national patents.

WALID EL-SHAFAI was born in Alexandria, Egypt. He received the B.Sc. degree (Hons.) in electronics and electrical communication engineering from the Faculty of Electronic Engineering (FEE), Menoufia University, Menouf, Egypt, in 2008, the M.Sc. degree from the Egypt–Japan University of Science and Technology (E-JUST), in 2012, and the Ph.D. degree from FEE, Menoufia University, in 2019. Since January 2021, he has been a Postdoctoral Research Fellow with the Security Engineering Laboratory (SEL), Prince Sultan University (PSU), Riyadh, Saudi Arabia. He is currently a Lecturer and an Assistant Professor with the Department of Electronics and Communication Engineering (ECE), FEE, Menoufia University. His research interests include wireless mobile and multimedia communications systems, image and video signal processing, efficient 2-D video/3-D multi-view video coding, multi-view video plus depth coding, 3-D multi-view video coding and transmission, quality of service and experience, digital communication techniques, cognitive radio networks, adaptive filters design, 3-D video watermarking, steganography, encryption, error resilience and concealment algorithms for H.264/AVC, H.264/MVC, and H.265/HEVC video codecs standards, cognitive cryptography, medical image processing, speech processing, security algorithms, software-defined networks, the Internet of Things, medical diagnoses applications, FPGA implementations for signal processing algorithms and communication systems, cancellable biometrics and pattern recognition, image and video magnification, artificial intelligence for signal processing algorithms and communication systems, modulation identification and classification, image and video super-resolution and denoising, cybersecurity applications, malware and ransomware detection and analysis, deep learning in signal processing, and communication systems applications. He also serves as a reviewer for several international journals.

NAGLAA F. SOLIMAN received the B.Sc., M.Sc., and Ph.D. degrees from the Faculty of Engineering, Zagazig University, Egypt, in 1999, 2004, and 2011, respectively. She worked with the Faculty of Computer Science, PNU, Saudi Arabia. Since 2015, she has been a Teaching Staff Member with the Department of Electronics and Communications Engineering, Faculty of Engineering, Zagazig University. Her current research interests include digital image processing, information security, multimedia communications, medical image processing, optical signal processing, big data, and cloud computing.